JEM Journal of Experimental Medicine

ARTICLE

Stage-specific action of Runx1 and GATA3 controls silencing of PU.1 expression in mouse pro–T cells

Hiroyuki Hosokawa[1,2,3], Maria Koizumi[1], Kaori Masuhara[1], Maile Romero-Wolf[3], Tomoaki Tanaka[4], Toshinori Nakayama[5], and Ellen V. Rothenberg[3]

PU.1 (encoded by *Spi1*), an ETS-family transcription factor with many hematopoietic roles, is highly expressed in the earliest intrathymic T cell progenitors but must be down-regulated during T lineage commitment. The transcription factors Runx1 and GATA3 have been implicated in this *Spi1* repression, but the basis of the timing was unknown. We show that increasing Runx1 and/or GATA3 down-regulates *Spi1* expression in pro–T cells, while deletion of these factors after *Spi1* down-regulation reactivates its expression. Leveraging the stage specificities of repression and transcription factor binding revealed an unconventional but functional site in *Spi1* intron 2. Acute Cas9-mediated deletion or disruption of the Runx and GATA motifs in this element reactivates silenced *Spi1* expression in a pro–T cell line, substantially more than disruption of other candidate elements, and counteracts the repression of *Spi1* in primary pro–T cells during commitment. Thus, Runx1 and GATA3 work stage specifically through an intronic silencing element in mouse *Spi1* to control strength and maintenance of *Spi1* repression during T lineage commitment.

Introduction

PU.1, encoded by *Spi1*, is an E twenty-six (ETS)–family transcription factor with multiple roles in the development and function of myeloid and lymphoid hematopoietic lineages (Carotta et al., 2010; Rothenberg et al., 2019; Singh et al., 1999). Expression levels of *Spi1* are highest in macrophages, granulocytes, and dendritic cells and moderate in lymphoid progenitors, reducing expression in B cells and turning off entirely in natural killer and T cells (Yoshida et al., 2019). Through pioneering-like activity and differential cofactor recruitment, PU.1 can control specification of several blood cell types (Heinz et al., 2010; Heinz et al., 2013; Hosokawa et al., 2018b; Ostuni et al., 2013; Rothenberg et al., 2019). Dysregulation of *Spi1* expression and translocation of the *Spi1* gene can induce malignant transformation in multiple hematopoietic lineages (Rosenbauer et al., 2004; Seki et al., 2017; Vangala et al., 2003). Thus, *Spi1* expression must be tightly regulated in a lineage-specific manner. *Spi1*-deficient hematopoietic stem cells fail to contribute to the T cell lineage in bone marrow (BM) chimera mice (Dakic et al., 2005; Scott et al., 1994), but *Spi1* expression must be shut off during T lineage commitment. The mechanism of this repression has remained obscure until now.

T cells develop from multipotent precursors in the thymus, where microenvironmental Notch signaling educates progenitors to become T cells (Hosokawa and Rothenberg, 2021; Radtke et al., 2013; Romero-Wolf et al., 2020). The earliest T progenitors in the thymus lack expression of the mature T cell markers CD4 and CD8 (double negative [DN]). The expression profiles of Kit, CD44, and CD25 in DN thymocytes distinguish developmental stages (Hosokawa et al., 2021; Hosokawa and Rothenberg, 2021; Rothenberg et al., 2008; Yang et al., 2010; Yui and Rothenberg, 2014). The earliest T cell precursors in the thymus, Kit^{hi} DN1 cells (here "DN1," $Kit^{hi+}CD44^{+}CD25^{-}$, or ETP), and their DN2a ($Kit^{hi+}CD44^{+}CD25^{+}$) descendants, still have access to non–T cell fates and proliferate to expand the intrathymic progenitor pool (Lu et al., 2005). They lose multipotency in transition from DN2a to DN2b ($Kit^{int+}CD44^{+}CD25^{+}$), becoming committed to the T lineage (Fig. 1 A). Next, TCRβ gene rearrangement at the DN3 ($Kit^{lo}CD44^{lo}CD25^{+}$) stage triggers pre-TCR–dependent progression to DN4 ($Kit^{lo}CD44^{lo}CD25^{-}$) and double-positive ($CD4^{+}CD8^{+}$) stages, leading to full TCR expression (Hosokawa and Rothenberg, 2018; Yui and Rothenberg, 2014).

The chromatin landscape and transcriptome profiles change dynamically at the transition from precommitment, DN1 and

[1]Department of Immunology, Tokai University School of Medicine, Isehara, Kanagawa, Japan; [2]Institute of Medical Sciences, Tokai University, Isehara, Kanagawa, Japan; [3]Division of Biology & Biological Engineering, California Institute of Technology, Pasadena, CA; [4]Department of Molecular Diagnosis, Graduate School of Medicine, Chiba University, Chuo-ku, Chiba, Japan; [5]Department of Immunology, Graduate School of Medicine, Chiba University, Chuo-ku, Chiba, Japan.

Correspondence to Ellen V. Rothenberg: evroth@its.caltech.edu; Hiroyuki Hosokawa: hosokawa.hiroyuki.g@tokai.ac.jp; M. Romero-Wolf's present address is Department of Stem Cell Biology and Regenerative Medicine, University of Southern California, Los Angeles, CA.

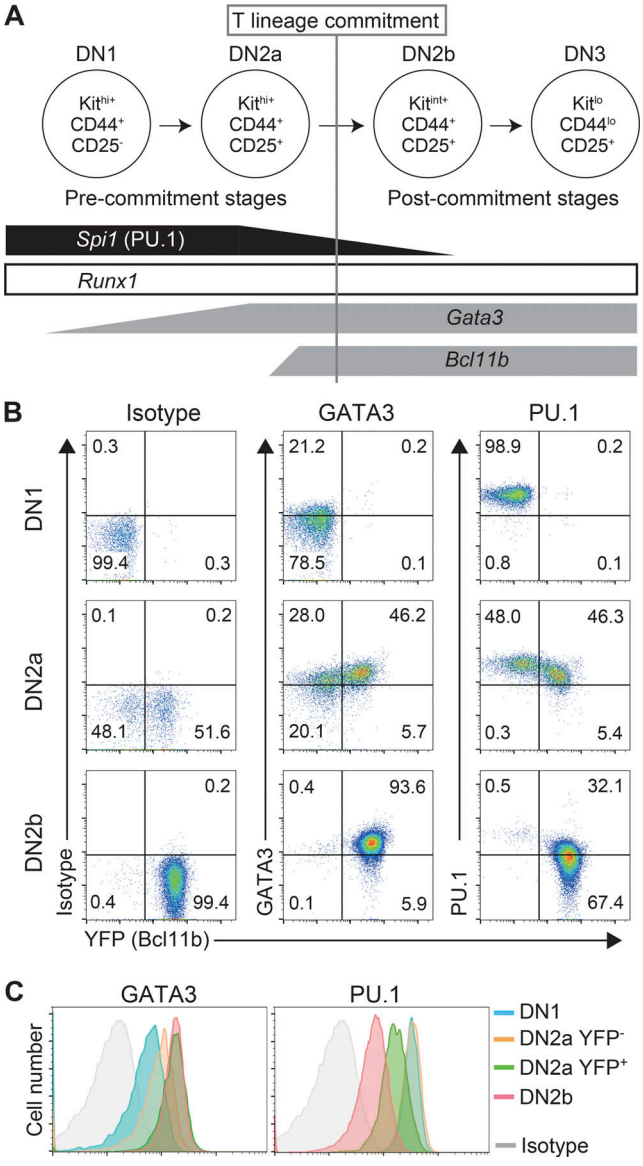

Figure 1. **Expression profiles of GATA3, PU.1, and Bcl11b around the T lineage commitment checkpoint. (A)** Schematic of early T cell development is shown with expression kinetics of the transcription factors *Spi1* (PU.1), *Runx1*, *Gata3*, and *Bcl11b*. **(B)** Intracellular staining for GATA3 and PU.1 was performed using DN thymocytes from Bcl11b-YFP reporter mice, gated as in Fig. S1 A. Representative profiles of isotype control (left), GATA3 (middle), and PU.1 (right) with Bcl11b-YFP in DN1, DN2a, and DN2b are shown with the percentages of cells in each quadrant. Results are representative of three independent experiments. **(C)** Intracellular staining profiles of GATA3 (left) and PU.1 (right) in DN1, DN2a-YFP$^-$, DN2a-YFP$^+$, and DN2b are shown. The gray-filled histogram shows isotype control staining. GATA3, DN2a YFP$^+$ and DN2b curves overlap; PU.1, DN1 and DN2a YFP$^-$ curves overlap. Results are representative of three independent experiments.

DN2a, pro–T cells to T lineage–committed, DN2b and DN3, pro–T cells (Hosokawa et al., 2021; Hosokawa and Rothenberg, 2021; Hu et al., 2018). Two transcription factors, PU.1 and Bcl11b, change expression reciprocally in this process. While *Bcl11b* turns on as cells undergo commitment (Kueh et al., 2016; Zhou et al., 2019), *Spi1* is shut off during T lineage commitment, eliminating access to myeloid programs (Hosokawa et al., 2021; Hosokawa and Rothenberg, 2018; Yui and Rothenberg, 2014; Fig. 1 A). Conditional deletion of the *Spi1* gene before commitment not only causes faster developmental progression but also reduces cell yield (Champhekar et al., 2015; Hosokawa et al., 2018b). Thus, PU.1 supports the expansion of the uncommitted DN1 and DN2a T progenitor pool (Hosokawa and Rothenberg, 2021). However, inefficient repression or abnormal activation of *Spi1* after T lineage commitment can yield malignancy, directly or via its target genes (Boehm et al., 1991; Homminga et al., 2011; Hosokawa and Rothenberg, 2021; Rosenbauer et al., 2006; Seki et al., 2017; Yui and Rothenberg, 2014).

Regulatory mechanisms controlling *Spi1* expression kinetics during early T cell development are not fully understood. Multiple reports have suggested roles for Runx1 and GATA3 as mediators of *Spi1* repression in mouse pro–T cells. When *Runx1* was deleted conditionally by Mx1-Cre activation in mice, early T cell development was significantly blocked at precommitment stages with increased *Spi1* expression (Growney et al., 2005; Huang et al., 2008), and *Runx1* deletion in pro–T cells developing in vitro also caused *Spi1* up-regulation (Hosokawa et al., 2018b). GATA3 overexpression severely repressed *Spi1* in fetal pro–T cells (Taghon et al., 2007), while shRNA knockdown of *Gata3* caused up-regulation of *Spi1* in fetal thymus- or liver-derived pro–T cells (Scripture-Adams et al., 2014). However, *Runx1* and *Gata3* perturbation in progenitor cells also strongly reduces pro–T cell yields, and their expression increases little during commitment. Thus, how Runx1 and GATA3 cause this stage-specific *Spi1* repression has remained uncertain.

Multiple cis-regulatory elements around the *Spi1* locus could play roles. The promoter, a major upstream regulatory element (URE), and conserved noncoding element 4 (CE4) and CE5 have all been suspected to play roles in cell type–specific regulation of *Spi1* in myeloid, B, and T cells (Hoogenkamp et al., 2007; Li et al., 2001; Okuno et al., 2005; Rosenbauer et al., 2006; Rosenbauer et al., 2004; Zarnegar et al., 2010). The URE, a highly conserved noncoding genomic region 14 kb upstream of the transcriptional start site of *Spi1* (–14 kb; Li et al., 2001; Okuno et al., 2005), showed enhancer activity in myeloid and B cells (Rosenbauer et al., 2006; Rosenbauer et al., 2004), while its T lineage role appeared bivalent or repressive (Hoogenkamp et al., 2007; Huang et al., 2008; Montecino-Rodriguez et al., 2018; Zarnegar et al., 2010). URE KO mice showed a partial defect in early T cell development, characterized by increased *Spi1* expression in DN1 as well as DN3 stages of adult mice (Rosenbauer et al., 2006). Thus, the bifunctional URE region can damp *Spi1* expression in pro–T cells, but whether it explains the switch to repression is less clear. CE4 and CE5, upstream (–9.2 and –10.3 kb) conserved noncoding regions, were identified as T cell–specific silencer and myeloid-specific enhancer elements using reporter assays with cell lines (Zarnegar et al., 2010). However, CE4 element function has not been demonstrated in its native context.

Here, we describe a new regulatory element through which GATA3 and Runx1 appear to work stage specifically to silence *Spi1* in T lineage commitment. Using pro–T cell differentiation cultures with acute, stage-specific perturbations, we verify roles and structural requirements of GATA3 and Runx1 for *Spi1* repression. Highly stage-specific binding of Runx1 and GATA3 in

pro–T cells during commitment identifies a *Spi1* intronic site that is functionally important for the magnitude and maintenance of *Spi1* repression in a pro–T cell line and primary pro–T cells, with greater impact than CE4 or other candidate repression elements. Taken together, this evidence identifies a direct mechanism through which Runx1 and GATA3 mediate the stage-specific repression of *Spi1*.

Results

Runx1 and GATA3 protein expression relative to *Spi1* expression around T lineage commitment

Gata3 turns on soon after precursors enter the thymus, reaching a plateau in late DN2a stage (Yoshida et al., 2019; Zhou et al., 2019; Fig. 1 A). Pro–T cells express *Runx1* more highly than other hematopoietic cell types (Yoshida et al., 2019), and both Runx1 mRNA and protein are highest across commitment (Shin et al., 2021; Zhou et al., 2019). In DN pro–T cells, shortly before *Spi1* expression decreases, expression of *Gata3* and *Runx1* mRNA increases slightly (Yoshida et al., 2019; Zhang et al., 2012).

To determine whether GATA3 protein levels could be rate limiting for PU.1 silencing in early pro–T cells, we conducted intracellular staining for GATA3 and PU.1. We used thymocytes from Bcl11b-YFP reporter mice (Kueh et al., 2016) to monitor Bcl11b up-regulation, marking T lineage commitment in late DN2a stage (Fig. 1 A), and compared DN1 ($Kit^{hi+}CD25^{-}$), DN2a ($Kit^{hi+}CD25^{+}$), and DN2b ($Kit^{int+}CD25^{+}$) stages among the DN, $Lin^{-}CD44^{+}Kit^{+}$ thymocytes (Fig. S1 A). The results (Fig. 1, B and C) confirmed that GATA3 levels were very low in the DN1 stage, slightly up-regulated in the DN2a $Bcl11b^{-}$ (YFP^{-}) stage, and further increased in the DN2a $Bcl11b^{+}$ (YFP^{+}) and DN2b stages. PU.1 was highly expressed in the DN1 and DN2a $Bcl11b^{-}$ stages but then shifted lower in DN2a cells as they began to express Bcl11b (Fig. 1, B and C) and had clearly dropped by DN2b stage (cf. Ungerbäck et al., 2018; Yui et al., 2010). Given the high protein stability of PU.1 (Kueh et al., 2013), the slight reduction seen in $Bcl11b^{+}$ DN2a cells is consistent with the onset of repression. In separate work (Shin et al., 2021), we found that Runx1 protein also detectably increased from the DN1 to DN2a/b stages. Thus, GATA3 and Runx1 protein levels beyond a certain threshold could influence the timing of PU.1 repression.

Transduction of *Runx1* and *Gata3* represses *Spi1* expression in precommitment pro–T cells

To verify whether Runx1 and/or GATA3 levels control *Spi1* expression in pro–T cells, we tested whether their overexpression in DN1 and DN2a pro–T cells could accelerate the natural silencing of *Spi1*. Runx and GATA3 perturbations are demonstrably toxic in vitro, leaving some uncertainty as to whether gene-expression changes seen in previous studies reflected direct gene regulation or population selection (Guo et al., 2008; Huang et al., 2008; Scripture-Adams et al., 2014; Taghon et al., 2007; Telfer et al., 2004). We used BM progenitor cells from *Bcl2* transgenic (Tg) mice to maximize viable recovery, culturing them on OP9 Delta-like 1 (DLL1; a Notch ligand) stroma to initiate T cell development in vitro (see Materials and methods). On day 3 of culture, when most of the cells were still in precommitment stages (DN1 and DN2a), they were infected with retroviral vectors expressing *Runx1* and/or *Gata3* with GFP or human nerve growth factor receptor (hNGFR) markers, respectively. We sorted $Lin^{-}CD45^{+}CD44^{+}GFP^{+}hNGFR^{+}$ precommitment cells for analysis at 3 d postinfection (dpi; day 6 of culture overall; Fig. 2, A and B; and Fig. S1 B; protocol A). Introduction of *Gata3* into these precommitment cells, which still had high *Spi1* expression, profoundly repressed *Spi1*, while *Runx1* transduction had a moderate but consistent effect. The combination of *Runx1* and *Gata3* introduction further intensified repression of *Spi1* (Fig. 2 C). In contrast, while *Spi1* down-regulation coincided most closely with the timing of Bcl11b-YFP activation during development, overexpression of *Bcl11b* did not repress *Spi1* expression (Fig. S1 C). This supports previous indications that Bcl11b does not itself regulate *Spi1* in mouse pro–T cells (Hosokawa et al., 2018a; Longabaugh et al., 2017).

Antisense transcripts from intron 3 of the *Spi1* locus reportedly act as negative modulators of *Spi1* expression (Ebralidze et al., 2008). Runx1 and GATA3 might reduce *Spi1* expression by stimulating expression of these antisense transcripts. However, precommitment cells with and without overexpression of *Runx1* and/or *Gata3* had comparable ratios of sense and antisense transcripts of exon3 of the *Spi1* gene (Fig. S1 D). Therefore, *Spi1* repression by Runx1 and GATA3 does not appear to be mediated by up-regulation of antisense transcripts of *Spi1* locus.

Structural requirements for GATA3 and Runx1 repression of *Spi1*

To test whether GATA3 might repress *Spi1* directly or whether it worked by inducing other repressors, we tested GATA3 mutants that can differentially affect function, localization, and organization of GATA3 complexes in type 2 T helper and type 2 innate lymphoid cells (Furusawa et al., 2013; Hosokawa et al., 2015; Hosokawa et al., 2016; Hosokawa et al., 2013a; Hosokawa et al., 2013b; Yamagata et al., 2000). Phosphorylation of GATA3 at S308, T315, and S316 inhibits its repressive action by dissociating histone deacetylase 2 (HDAC2) from the GATA3–nucleosome remodeling and deacetylase (NuRD) complex (Hosokawa et al., 2016; Hosokawa et al., 2013b) and can be mimicked by a triple phospho-mimetic mutant (GATA3 3D). Transcriptional activity of GATA3, in contrast, associates with methylation of R261 (Hosokawa et al., 2015). Here, whereas phospho-deficient (GATA3 3A), methylation-mimicking (GATA3 R261F) and methylation-deficient (GATA3 R261K) mutants (Hosokawa et al., 2015; Hosokawa et al., 2016) all repressed *Spi1* similarly to GATA3 WT in precommitment, primary pro–T cells, the GATA3 3D mutant caused only minimal *Spi1* repression (Fig. 2 D). This suggests that unphosphorylated GATA3 itself is directly involved in the repression mechanism.

Intact Runx1 was also needed to maintain repression, at least in the Scid.adh.2c2 line, a postcommitment pro–T cell that normally does not express *Spi1* (Dionne et al., 2005; Hosokawa et al., 2018b). A strongly DNA-binding, truncated form of Runx (Runx1DN) lacking transactivation and repression domains competitively blocks both repression (Telfer et al., 2004) and activation (Hosokawa et al., 2018b) by endogenous Runx factors. Overexpression of full-length Runx1 in Scid.adh.2c2 cells did not

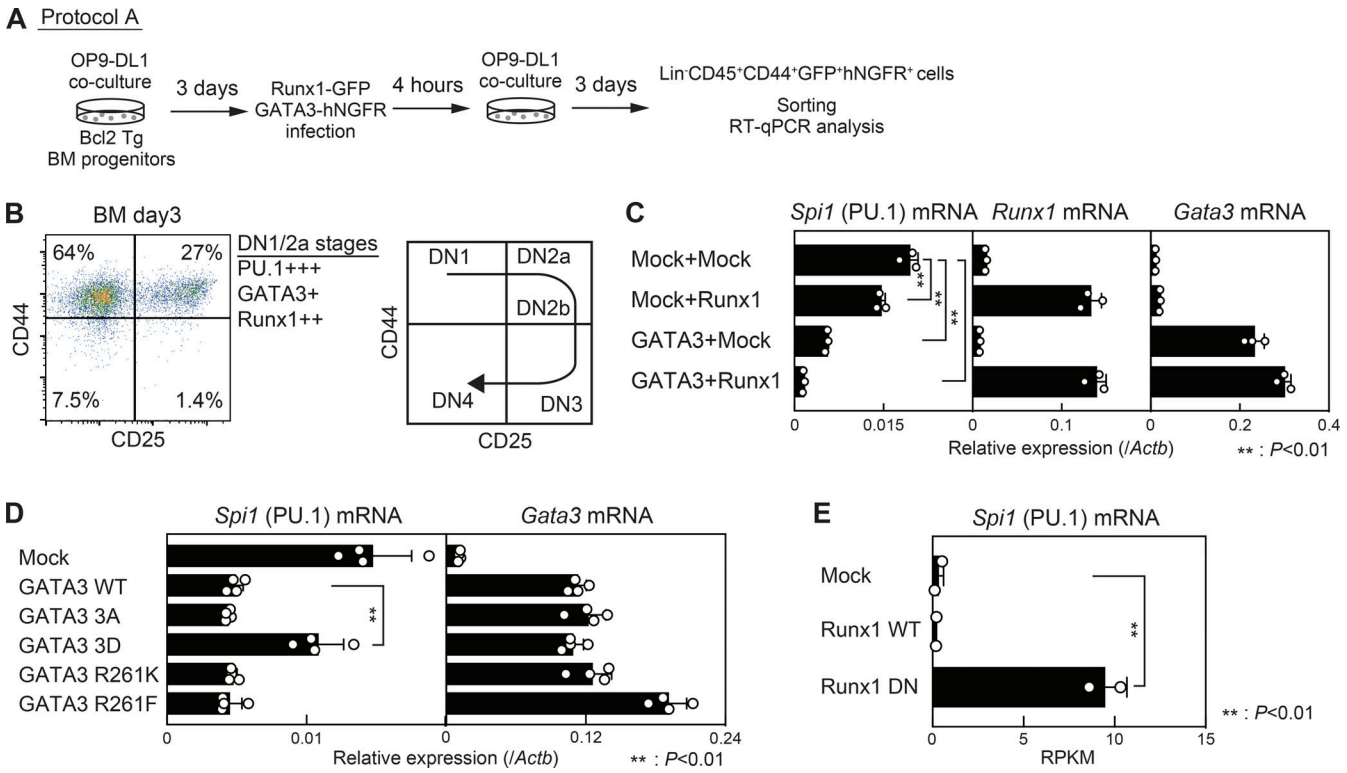

Figure 2. **Introduction of *Runx1* and *Gata3* represses *Spi1* expression in precommitment stages. (A)** An experimental scheme for introduction of *Runx1* and/or *Gata3* in precommitment pro–T cells is shown (protocol A). **(B)** BM progenitors obtained from Bcl2 Tg mice were co-cultured on OP9-DLL1. Flow cytometric analysis of T progenitors was performed on day 3, before retrovirus infection. A representative CD44/CD25 profile in Lin$^-$CD45$^+$ cells is shown (left). Schematic of the pro–T cell development trajectory is shown (right). Results are representative of three independent experiments. **(C)** Retrovirus-infected Lin$^-$CD45$^+$CD44$^+$GFP$^+$hNGFR$^+$ precommitment cells were sorted at 3 d after introduction. Expression levels of *Spi1* (left), *Runx1* (middle), and *Gata3* (right) were analyzed by RT-qPCR. The relative expression (/*Actb*) is shown with SD. **, P < 0.01 by two-sided Student's *t* test. Data are representative of two independent experiments and based on three biological replicates. **(D)** Precommitment cells were introduced with GATA3 WT, phospho-deficient (3A), phospho-mimic (3D; Hosokawa et al., 2016; Hosokawa et al., 2013b), methylation-deficient (R261K), or methylation-mimic (R261F) GATA3 mutants (Hosokawa et al., 2015; Nakayama et al., 2017) as protocol A. Expression levels of *Spi1* (left) and *Gata3* (right) were analyzed by RT-qPCR on 3 d after introduction. The relative expression (/*Actb*) is shown with SD. **, P < 0.01 by two-sided Student's *t* test. Data are representative of two independent experiments and based on four biological replicates. **(E)** Reads per kilobase per million reads (RPKM) values for *Spi1* in WT or DN form of *Runx1* introduced DN3-like cell lines are shown with SD (Hosokawa et al., 2018b).

alter the fully silent state of *Spi1*. However, introduction of the Runx1DN mutant caused endogenous *Spi1* to become activated, disrupting the established silent state (Fig. 2 E). Thus, the ability of Runx1 to recruit other protein partners via non-DNA-binding domains is crucial for maintenance of *Spi1* repression.

To identify the functional components of GATA3 complexes that control PU.1 repression in pro–T stages, we transduced Scid.adh.2c2 cells with Myc- and Flag-tagged GATA3 and recovered GATA3 complexes by two-step affinity purification followed by SDS-PAGE and silver staining (Fig. S1 E). Analysis by liquid chromatography and tandem mass spectrometry identified more than 150 molecules annotated as being involved in transcription or chromatin remodeling (Fig. S1 F and Table S1, sheet 1). While multiple subunits for the NuRD and BRG1-assocated factor (BAF) complexes were repeatedly detected, Runx1 had one of the highest signals in our mass spectrometry analyses, consistently in four separate samples (Table S1, sheet 2). The association between GATA3 and Runx1 was validated by coimmunoprecipitation with immunoblotting. Notably, even the GATA3 3D mutant (Fig. 2 D) was fully able to interact with Runx1, similarly to GATA3 WT and 3A mutant (Fig. S1 G), indicating that altered GATA3 activity itself caused by the 3D mutation accounted for its loss of repressive activity for *Spi1*.

Stage-specific deletion of *Runx1* and *Gata3* derepresses *Spi1* in committed pro–T cells

To confirm the role of natural levels of Runx1 and GATA3 expression in *Spi1* repression, we performed acute, stage-specific *Runx1* and *Gata3* disruption in primary cells after T lineage commitment using bicistronic retroviral vectors carrying sgRunx1 or sgGATA3 with CFP or hNGFR markers, respectively. These constructs induced acute, specific losses of the targeted proteins as detected by immunoblotting when transduced into Cas9-expressing Scid.adh.2c2 cells (Fig. S2 A). To test their impact in primary cells, BM progenitor cells from Cas9;Bcl2 Tg mice were co-cultured on OP9-DLL1 for 10 d, until nearly all cells had undergone commitment, and then they were transduced with the single guide RNA (sgRNA) against *Runx1* and/or *Gata3*, using control sgRNA transductions for comparison (Fig. 3, A and B; protocol B). 4-dpi, doubly transduced, postcommitment

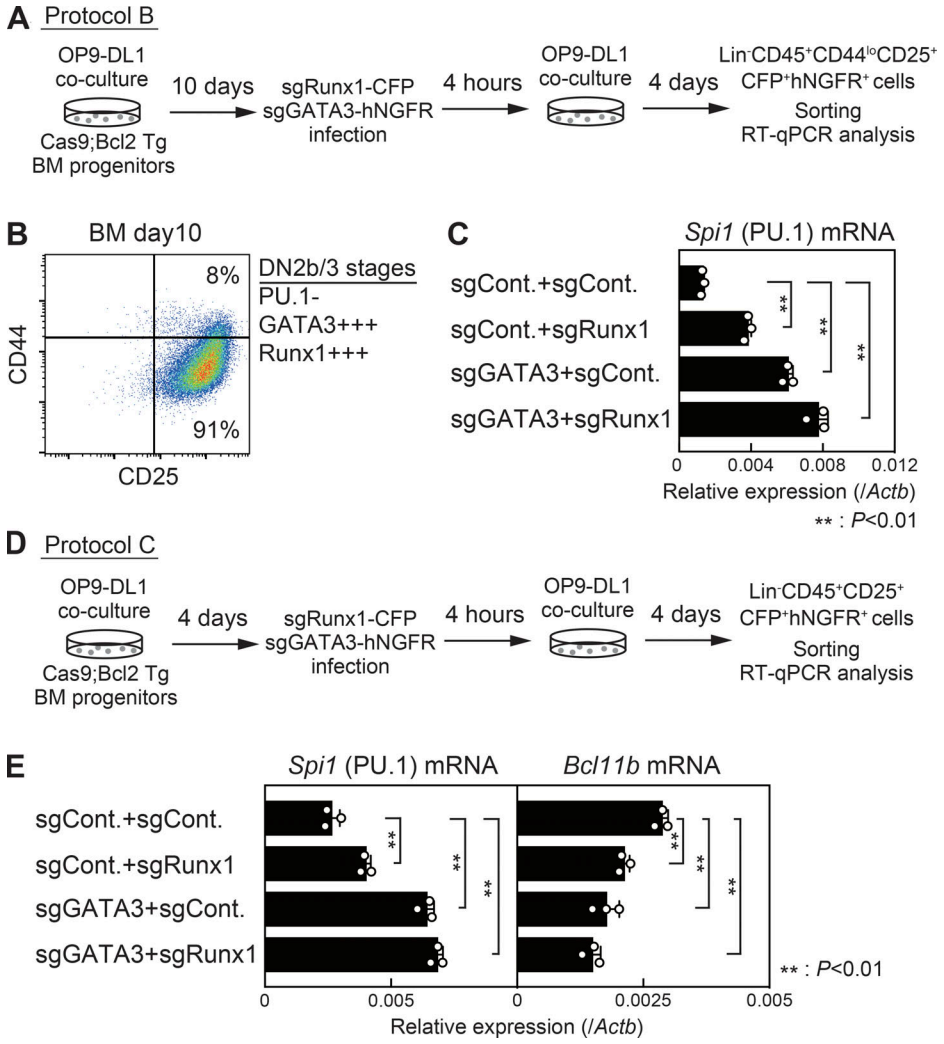

Figure 3. **Deletion of *Runx1* and *Gata3* induces derepression of *Spi1* expression in T lineage–committed cells. (A)** BM progenitors obtained from Cas9; Bcl2 Tg mice were co-cultured on OP9-DLL1 for 10 d. Postcommitment cells were retrovirally introduced sgRNAs against *Runx1* and/or *Gata3* and then analyzed 4 dpi (protocol B). **(B)** Flow cytometric analysis of BM-derived pro–T cells was performed on day 10, before sgRNA introduction. A representative CD44/CD25 profile in Lin⁻CD45⁺ cells is shown. The result is representative of three independent experiments. **(C)** sgRNA-introduced Lin⁻CD45⁺CD25⁺CD44ˡᵒCFP⁺hNGFR⁺ postcommitment cells were sorted and subjected to RT-qPCR analysis at 4 d after sgRNA introduction. The relative expression (/*Actb*) of *Spi1* is shown with SD. **, P < 0.01 by two-sided Student's *t* test. Data are representative of two independent experiments and based on three biological replicates. **(D)** BM progenitors were co-cultured on OP9-DLL1 for 4 d. Precommitment cells were retrovirally introduced sgRNAs against *Runx1* and/or *Gata3* and then analyzed 4 dpi (protocol C). **(E)** sgRNA-introduced Lin⁻CD45⁺CFP⁺hNGFR⁺ cells (D) were sorted and subjected to RT-qPCR analysis. The relative expression (/*Actb*) of *Spi1* and *Bcl11b* is shown with SD. **, P < 0.01 by two-sided Student's *t* test. Data are representative of two independent experiments and based on three biological replicates.

Lin⁻CD45⁺CD44ˡᵒCD25⁺CFP⁺hNGFR⁺ cells were sorted (Fig. S2 B), followed by RT quantitative PCR (RT-qPCR) analysis for *Spi1* mRNA (Fig. 3 C). Expression of *Spi1*, which is normally low in these committed cells, was substantially up-regulated by *Runx1* or *Gata3* KO, and combined loss of *Runx1* and *Gata3* up-regulated *Spi1* even more (Fig. 3 C). Earlier *Runx1* and *Gata3* deletion, around the time of T lineage commitment, had a similar effect. The deletion was initiated at day 4 (before T lineage commitment) and harvested on day 8 overall (Fig. 3 D; protocol C), in transition from DN2a to DN2b/DN3 (Fig. S2 C). Again, mRNA levels of *Spi1* were clearly higher in *Runx1* and/or *Gata3* KO cells than in controls. This up-regulation was specific for *Spi1*, because *Bcl11b*, a positive target of GATA3 and Runx1 (Kueh et al., 2016), showed the opposite pattern (Fig. 3 E). Thus, normal endogenous Runx1 and GATA3 are important for both establishing and maintaining repression of *Spi1* in the T cell lineage commitment transition.

DN2b/3 stage-specific binding of Runx1 and GATA3 at the intronic region of the *Spi1* locus

Multiple cis-regulatory elements have been described around the *Spi1* locus, especially evolutionarily conserved open chromatin regions, that reportedly control levels of *Spi1* expression in various hematopoietic cell types, as discussed in the Introduction. In an unbiased search for genomic sites that could mediate active imposition of repression during commitment, we

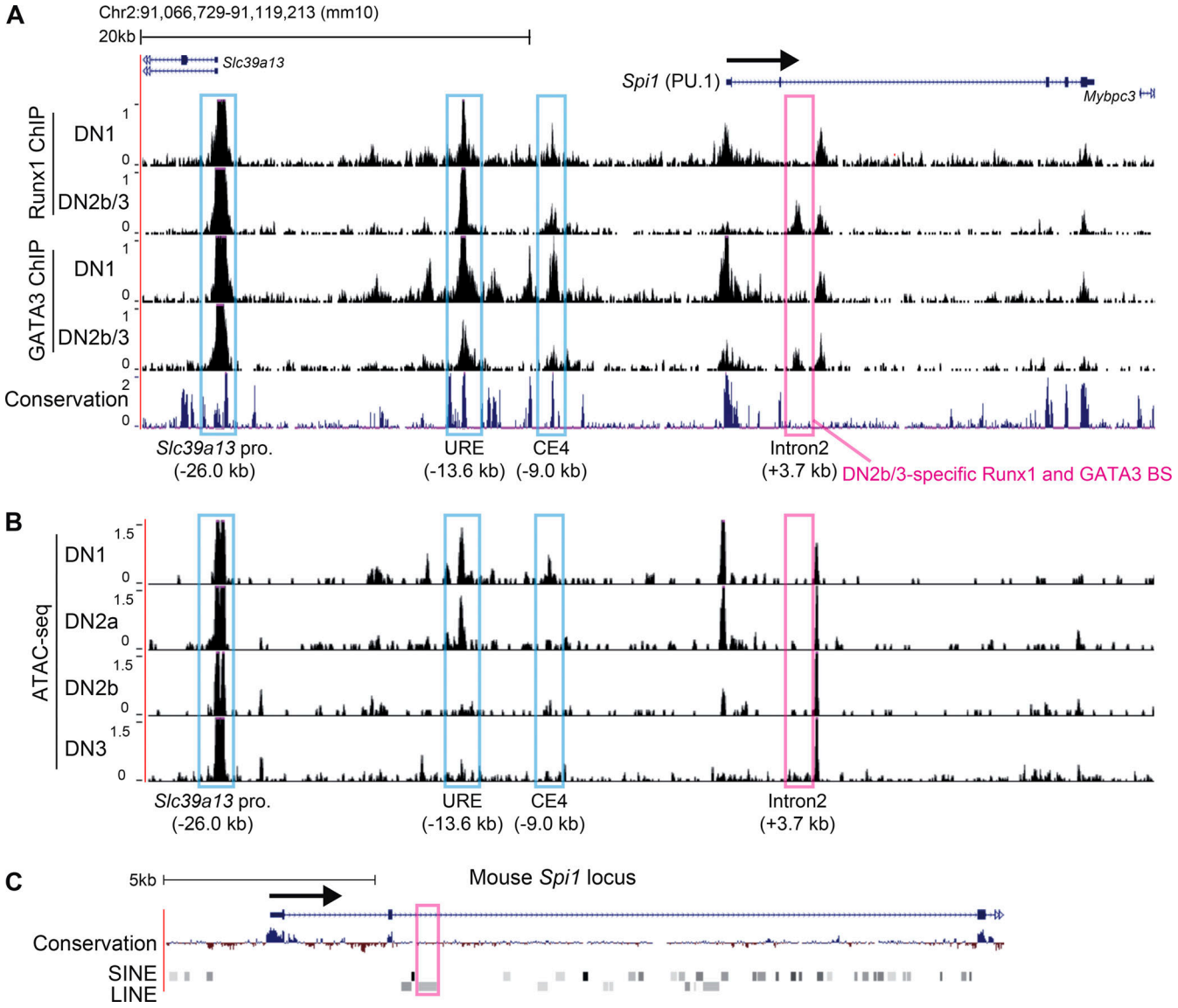

Figure 4. **Identification of the DN2b/3-specific Runx1 and GATA3 binding site at the *Spi1* locus. (A)** BM progenitors obtained from B6 mice were co-cultured on OP9-DLL1 for 5 or 14 d. Lin$^-$CD45$^+$CD25$^-$Kit^{hi+}CD44$^+$ DN1 cells and Lin$^-$CD45$^+$CD25$^+$Kit^{lo}CD44^{lo} DN2b/3 cells were sorted on days 5 and 14, respectively, and subjected to ChIP-seq analysis for Runx1 (Hosokawa et al., 2018b) and GATA3. Representative ChIP-seq tracks in DN1 and DN2b/3 cells around the *Spi1* locus are shown with the conservation track. Previously reported cis-regulatory elements and a DN2b/3-specific Runx1 and GATA3 binding site are labeled with blue and magenta rectangles, respectively. Data are representative of two independent experiments. Chr2, chromosome 2. **(B)** Representative ATAC-sequencing tracks in DN1, DN2a, DN2b and DN3 cells around the *Spi1* locus are shown (Yoshida et al., 2019). **(C)** The short interspersed nuclear element (SINE) and LINE element tracks around the *Spi1* locus in mouse (mm10) are shown with the conservation track. A position for the DN2b/3-specific Runx1 and GATA3 binding site is labeled with a magenta rectangle.

examined Runx1 and GATA3 binding around *Spi1* by chromatin immunoprecipitation (ChIP) and deep sequencing (ChIP-seq). We compared their occupancy patterns before (DN1) and after (DN2b/3) T lineage commitment (Hosokawa et al., 2018b; Fig. 4 A) and compared these with sites changing chromatin accessibility (Yoshida et al., 2019) and looping interactions (Hu et al., 2018) around *Spi1* in pre- and postcommitment pro–T cells (Fig. S3, A and B). Despite the strong impact of endogenous GATA3 on *Spi1*, conventional ChIP-seq conditions using formaldehyde (FA) crosslinking showed little, if any, GATA3 binding near this locus (Fig. S3 A). However, using a di(N-succinimidyl) glutarate (DSG) cross-linker that stabilizes Runx1-containing complexes (Hosokawa et al., 2020; Hosokawa et al., 2018b), GATA3 recruitment was clear (Fig. 4 A; see Materials and methods). Runx1 and GATA3 were found at URE, CE4 (Huang et al., 2008; Zarnegar et al., 2010), and the transcriptional start site of the neighboring *Slc39a13* gene. However, none of these peaks appeared after commitment (Fig. 4 A, blue rectangles). A site at −17.8 kb previously reported to mediate repression by GATA1 in erythroid cells (Chou et al., 2009) showed slight binding, but only in DN1 cells, not DN2b/3 cells.

Notably, however, we saw a small but reproducible peak of Runx1 and GATA3 association at +3.7 kb within intron 2 of *Spi1*, and these signals were highly DN2b/3-stage specific (Fig. 4 A,

magenta rectangle). Runx1 and GATA3 were also detected here in Scid.adh.2c2 cells (Fig. S3 C). Despite the modest signals, this site was the only one in the gene-to-gene interval containing *Spi1* (*Slc39a13-Mybpc3*) that showed DN2b/DN3-specific occupancy by Runx1 or GATA3. The sequence of this region included multiple Runx motifs and a GATA motif (see below). Runx1, at least, appeared to bind to this site independently of GATA3, as shown by acute knockouts and ChIP-qPCR assays (Fig. S4 A).

Interestingly, this site would not have been identified by assay of transposase-accessible chromatin (ATAC) accessibility or conservation. The URE and CE4 regions are ATAC accessible in DN1 stage and gradually close during pro–T progression, and a neighboring intron 2 site (at +5.0 kb) appears constitutively open. But the +3.7-kb site of the *Spi1* locus appears "closed" both before and after commitment (Yoshida et al., 2019; Fig. 4 B, magenta rectangle). This region also falls within a long interspersed nuclear element (LINE element; Fig. 4 C, magenta rectangle). Still, this site was close to the intron 2 anchor for a chromatin looping interaction that appears newly during commitment (Fig. S3 B, dark blue star).

Potential silencer activity of the DN2b/3-specific Runx1 and GATA3 binding site in the *Spi1* locus

To test whether the DN2b/3-specific Runx1 and GATA3 binding site at +3.7 kb of the *Spi1* locus could actually mediate Runx1- and GATA3-dependent silencer activity, we designed sgRNAs to disrupt the DN2b/3-specific Runx1 and GATA3 occupancy region and tested their impact first in the Scid.adh.2c2 pro–T cell line. Scid.adh.2c2 cells expressing Cas9-GFP were retrovirally transduced in parallel with pairs of sgRNAs flanking each of four different Runx1 and GATA3 binding regions around the *Spi1* locus. Besides the +3.7-kb region, we targeted the URE, CE4, and the neighboring *Slc39a13* promoter (*Slc39a13* pro.). Cas9$^+$ doubly transduced (GFP$^+$ CFP$^+$ hNGFR$^+$) cells were cloned by single-cell sorting (Fig. 5 A), and we identified clones with complete loss of the targeted genomic regions by genomic qPCR analysis (Fig. 5 B). Deletion of 567 bp of the +3.7-kb site (sgInt.2) induced markedly up-regulated *Spi1* expression in Scid.adh.2c2 cells (Fig. 5 C). In contrast, expression levels of *Spi1* were comparable among cells transduced with sgControl (sgRNA against luciferase), sgSlc39a13 promoter, and sgURE, whereas disruption of CE4 (sgCE4) led to only a slight increase in *Spi1* expression (Fig. 5 C). Therefore, in this DN3-like cell line, the DN2b/3-specific Runx1 and GATA3 binding site at +3.7 kb of the *Spi1* locus was required to maintain repression of *Spi1*.

Because GATA3 binding to the +3.7-kb element seemed weak, we examined the wider *Spi1* locus neighborhood for any additional sites where GATA3 binding increased from DN1 to DN2b/3. Of special interest were potential downstream anchor sites for the commitment-associated looping noted above (Fig. S3 B). Indeed, elements at +145 kb and +211 kb showed higher GATA3 binding signals in DN2b/3 stages than DN1 (Fig. S4 B), and another strong GATA3 peak near the potential loop anchor was seen at +167 kb. All three showed Runx1 and GATA3 co-occupancy in postcommitment cells with various degrees of stage specificity. In direct tests, disruption of the +145-kb genomic region induced weak but reproducible derepression of *Spi1* in Scid.adh.2c2 clones (Fig. S4, C and D), similar to CE4 disruption, whereas disruption of the +167-kb and +211-kb elements had no effect. Therefore, Runx1 and GATA3 may be involved in establishment of stage-specific repressive chromatin looping architectures around the *Spi1* locus, including the +3.7-kb, +145-kb, and CE4 elements.

Roles of Runx and GATA motifs in the DN2b/3-specific Runx1 and GATA3 binding site in PU.1 repression in primary pro–T cells

In primary pro–T cells, clones could not be grown out and selected for deletion of the complete element, but a Cas9-mediated point mutation strategy could be highly effective to test the role of the +3.7-kb element. There are three Runx motifs and one GATA motif around the center of the +3.7-kb element (Figs. 6 A and S5 A). Thus, we induced direct mutations in these Runx and GATA motifs at the +3.7-kb element in primary Cas9;Bcl2 Tg pro–T cells. Cells were cultured and transduced according to protocol B using sgRNAs targeting each motif (Fig. 6 A, red arrowheads) and analyzing the postcommitment, multiply transduced cells at day 14 overall (Fig. S5 B). Disruption of individual motifs had significant but minor effects on *Spi1* expression. In contrast, transduction of the mixture of sgRNAs against all four motifs induced prominent derepression of *Spi1* (Fig. 6 B), albeit not to full precommitment expression levels. PU.1 protein levels in individual cells were up-regulated throughout the population when all four motifs were disrupted (Fig. 6 C), while the cells introduced with the sgRNA mixture had individually undergone different combinations of point mutations or small deletions (Fig. S5 C).

Next, we tested whether the activity mediated by the +3.7-kb element is generally damping or stage specific. We disrupted all four Runx and GATA motifs early in the culture and then compared effects on *Spi1* levels expressed in precommitment stages (6 d) and later in postcommitment stages (12 d; Fig. 6 D; protocol D). Disruption with the four sgRNAs did not affect progression of DN stages, defined by CD44 and CD25 expression, and *Spi1* showed some developmental down-regulation in commitment in both experimental samples and controls (Fig. S5, D and E). However, the high expression of *Spi1* at 6 dpi (mostly DN2a/2b) was very similar in control and experimental samples, whereas by postcommitment stages at 12 dpi (DN2b/3, day 14 of overall culture), the four sgRNAs substantially alleviated *Spi1* repression compared with controls (Fig. 6 E). Thus, the intronic site of postcommitment stage-specific Runx1 and GATA3 binding was needed to strengthen or maintain repression of *Spi1* expression, stage specifically, after commitment.

Finally, to determine whether the +3.7-kb site was required to mediate repressive action of Runx1 or GATA3 on *Spi1*, we disrupted the four motifs in precommitment pro–T cells and then transduced the cells with *Runx1* or *Gata3* (Fig. 7 A; protocol E). Runx1- and GATA3-mediated repression of *Spi1* expression was significantly weakened in the cells transduced with the mixed sg4 motifs compared with controls (Fig. 7 B). Although introduction of *Gata3* was still able to cause some repression of *Spi1*, the attenuation of this effect via a single intronic element was notable considering not only the intact +145-kb and CE4 elements but also the multiple potent gene network impacts of

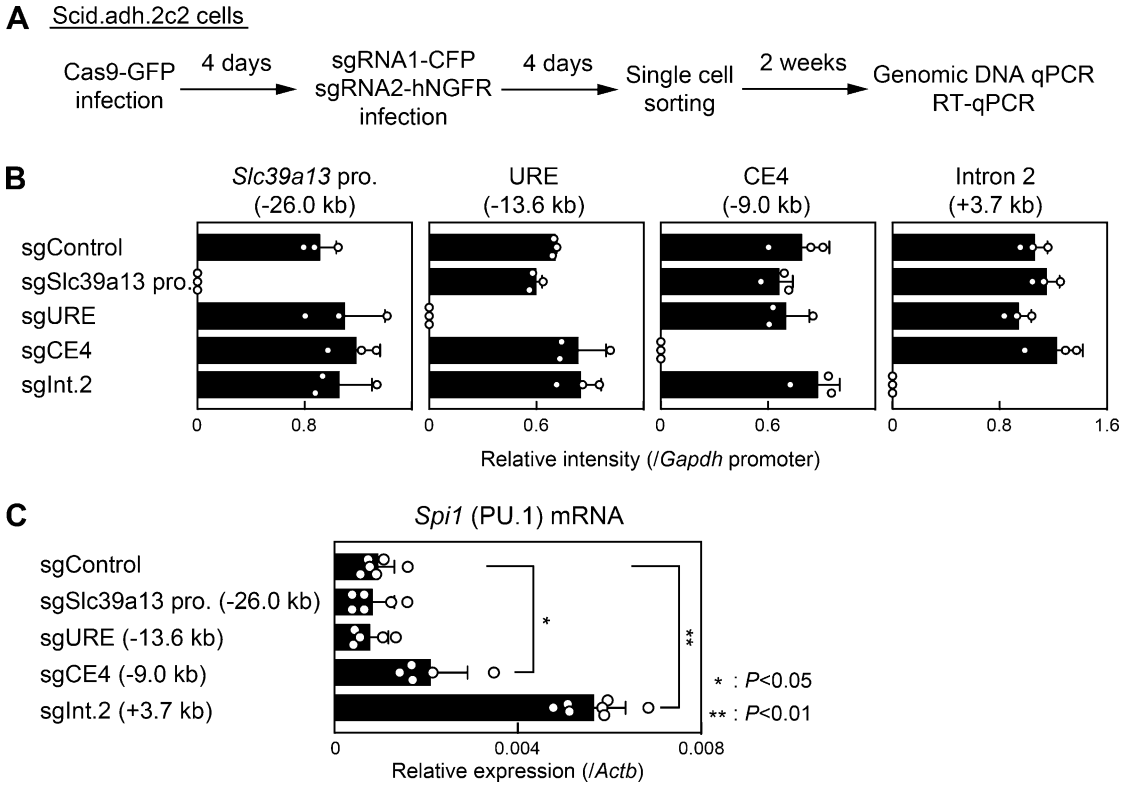

Figure 5. **Activation of *Spi1* is induced by deletion of the DN2b/3-specific Runx1 and GATA3 binding site in a DN3-like cell line. (A)** A DN3-like cell line, Scid.adh.2c2, was used for CRISPR-Cas9–mediated deletion of the specific genomic regions around *Spi1* locus. First, Scid.adh.2c2 cells were introduced Cas9-GFP, and then they were infected second retrovirus infection for sgRNAs against two sides of the targeted genomic regions. GFP⁺CFP⁺hNGFR⁺ cells were subjected to single-cell sorting and expanded for 2 wk. **(B)** Genomic DNA from each clone was isolated and subjected to qPCR analysis to confirm deletion of the targeted genomic regions. The relative intensity (/*Gapdh* promoter) is shown with SD. Data are based on three independent clones. **(C)** Relative expression levels of *Spi1* against *Actb* are shown with SD. Circles indicate independent clones. **, P < 0.01; *, P < 0.05 by two-sided Student's *t* test. Data are based on more than five independent clones.

Runx1 and GATA3 on other regulators in the cells (Scripture-Adams et al., 2014; Shin et al., 2021; Fig. 7 B). Taken together, postcommitment stage-specific binding of Runx1 and GATA3 to the +3.7-kb element of the *Spi1* locus may play a substantial role in timing of *Spi1* repression during early T cell development.

Discussion

PU.1 has an indispensable role for the earliest T lineage precursors in the thymus (Champhekar et al., 2015; Dakic et al., 2005), but its expression must be shut off during T lineage commitment, at the transition from DN2a to DN2b, and both the mechanism and coordination of this timing have needed explanation. Despite evidence that Runx1 and GATA3 play roles in the repression of *Spi1* in pro–T cells, possibly via the URE and other cis-regulatory elements around the *Spi1* locus (Huang et al., 2008; Rosenbauer et al., 2006; Scripture-Adams et al., 2014; Zarnegar et al., 2010), both Runx1 and GATA3 are expressed for many cell divisions before *Spi1* is silenced. Similarly, the chromatin accessibility and transcription factor binding dynamics at these previously reported genomic elements have failed to explain how *Spi1* expression is repressed specifically during pro–T cell lineage commitment. This problem motivated our search for new Runx1–GATA3–*Spi1* interactions that could mediate this stage-specific functional change. Here, we exploited CRISPR-Cas9–mediated acute, stage-specific deletions of *Runx1*, *Gata3*, and/or potential cis-regulatory elements in an in vitro T cell development culture system. We confirmed that precommitment overexpression of Runx1 and GATA3 markedly accelerated *Spi1* repression, whereas stage-specific deletion of *Runx1* and *Gata3* derepressed or significantly weakened repression of *Spi1*. Using stage-specific Runx1 and GATA3 binding as a search criterion, we identified a novel element in the second intron of *Spi1*, not described before, which was shown to mediate stage-specific silencer activity dependent on the integrity of Runx1 and GATA3 binding sites. While GATA3 and Runx1 binding to the previously described CE4 element (Zarnegar et al., 2010) and a far downstream element at +145 kb may also contribute, their effects were weaker in a cell line model. Disruption of the +3.7-kb element alone was sufficient to give *Spi1* at least 50% protection from the repressive effects of overexpressed GATA3 or Runx1. Thus, the repression of *Spi1* by Runx1 and GATA3 is controlled at least in part via their stage-specific binding to this *Spi1* intronic site.

The striking feature of Runx1 and GATA3 action in repression of *Spi1* has been the stage-specific functional response occurring with seemingly little change in levels of the two candidate repressive factors. However, both Runx factors and GATA3 have

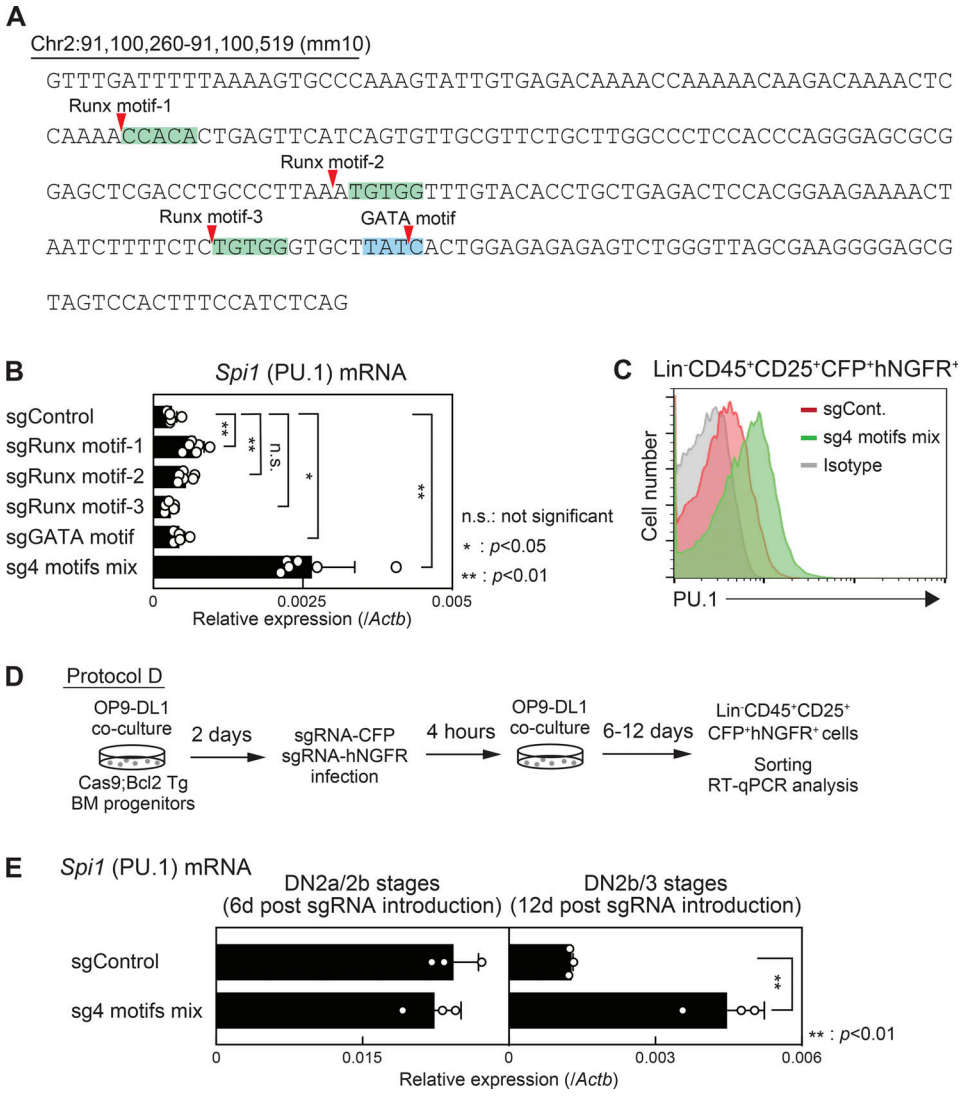

Figure 6. **Stage-specific derepression of *Spi1* is induced by mutations on the Runx and GATA motifs in the *Spi1* +3.7-kb element. (A)** The sequence of the DN2b/3-specific Runx1 and GATA3 binding site at intron 2 of the *Spi1* gene (chromosome 2; 91,100,260–91,100,519) is indicated. Runx motifs and a GATA motif are labeled with green and blue boxes, respectively. Red arrowheads indicate targeted sites for CRISPR-Cas9–mediated direct mutations. **(B)** sgRNA-introduced Lin$^-$CD45$^+$CD25$^+$CD44^{lo}CFP$^+$hNGFR$^+$ postcommitment cells were sorted and subjected to RT-qPCR analysis at 4 d after sgRNA introduction (protocol B). The relative expression (/*Actb*) of *Spi1* is shown with SD. **, P < 0.01; *, P < 0.05 by two-sided Student's *t* test. Data are representative of two independent experiments and based on more than five biological replicates. **(C)** sgControl- or sg4 motifs mix–introduced Lin$^-$CD45$^+$CD25$^+$CD44^{lo}CFP$^+$hNGFR$^+$ postcommitment cells were subjected to intracellular staining for PU.1, at 4 d after sgRNA introduction (protocol B). Representative profiles for PU.1 are shown with isotype control staining (gray). Results are representative of four independent experiments. **(D)** BM progenitors obtained from Cas9; Bcl2 Tg mice were co-cultured on OP9-DLL1 for 2 d. Precommitment cells were retrovirally introduced with sgRNAs and then analyzed 6 (DN2a/2b stages) or 12 (DN2b/3 stages) dpi (protocol D). For cell surface phenotypes, see Fig. S5 D. **(E)** sgRNA-introduced Lin$^-$CD45$^+$CD44$^+$CFP$^+$hNGFR$^+$ DN2a/2b cells (left) and Lin$^-$CD45$^+$CD25$^+$CD44^{lo}CFP$^+$hNGFR$^+$ DN2b/3 cells (right) were sorted on 6 or 12 d after sgRNA introduction, respectively, and subjected to RT-qPCR analysis. The relative expression (/*Actb*) of *Spi1* is shown with SD. **, P < 0.01 by two-sided Student's *t* test. Data are representative of two independent experiments and based on three biological replicates.

been noted for the shifting of their genomic binding site choices from one stage to another in pro–T cells (Hosokawa et al., 2021; Hosokawa et al., 2018b; Shin et al., 2021; Zhang et al., 2012). Runx1 protein expression levels increase little between pre-commitment DN2a and postcommitment DN2b stages (Shin et al., 2021), and recent data show that Runx3 actually collaborates with Runx1 to repress *Spi1* during commitment, with their combined activities virtually constant before and after *Spi1* repression begins (Shin et al., 2021). However, both factors show the same stage-specific increased binding to the +3.7-kb site during commitment (Shin et al., 2021). GATA3 protein levels do increase slightly during commitment, in a way well coordinated with the change in expression of PU.1, but seemingly by less than threefold. Thus, despite little absolute change in total Runx and GATA3, their repression of *Spi1* correlates with their occupancy of the +3.7-kb site, possibly connected with a new chromatin loop anchored in intron 2. Recruitment could depend on additional partners not yet defined.

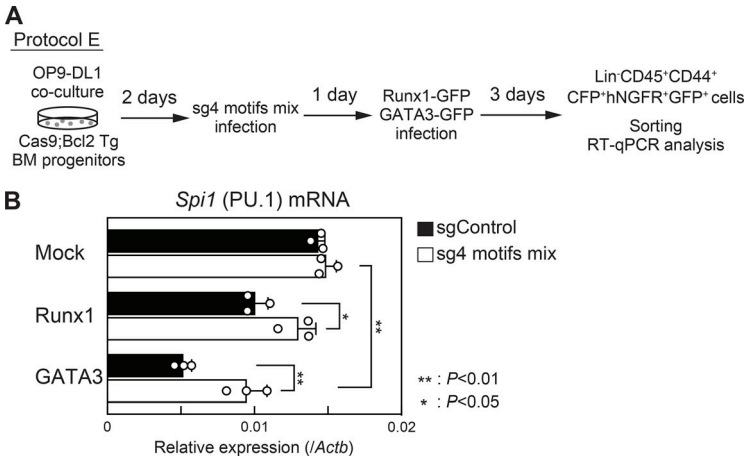

Figure 7. **Runx1 and GATA3 repress *Spi1* expression partly via the +3.7-kb element of the *Spi1* locus. (A)** BM progenitors obtained from Cas9;Bcl2 Tg mice were co-cultured on OP9-DLL1. Precommitment cells were retrovirally introduced with sg4 motifs mix on day 2, then with *Runx1* or *Gata3* on day 3. Retrovirus-transduced cells were analyzed 3 d after the last infection (protocol E). **(B)** Retrovirus-transduced Lin$^-$ CD45$^+$ CD44$^+$ CFP$^+$ hNGFR$^+$ GFP$^+$ cells were sorted on 3 d after introduction and subjected to RT-qPCR analysis as protocol E. The relative expression (/*Actb*) of *Spi1* is shown with SD. **, P < 0.01; *, P < 0.05 by two-sided Student's *t* test. Data are representative of two independent experiments and based on three biological replicates.

Deletion of *Runx1* and *Gata3* before T lineage commitment had stronger effects on progression of pro–T cell development and *Spi1* repression than deletion of the intronic stage-specific Runx1 and GATA3 target site. This could reflect additional repressive inputs from more distal regulatory sites, such as the +145-kb site near the distal end of a new commitment-associated loop, three to five genes away from the *Spi1* locus (Fig. S3 B; and Fig. S4, B–D). Repressive activity of GATA3 could also be unmasked if it undergoes signal-dependent dephosphorylation during commitment (Fig. 2 D). Alternatively, as Runx1 and GATA3 are critical regulators of multiple other genes, their levels could also influence *Spi1* expression via indirect mechanisms (Fig. 7 B). In principle, they could repress activators of *Spi1* such as *Cebpa* (Laiosa et al., 2006; Wang et al., 2006; Yeamans et al., 2007) and *Lmo2* (Cleveland et al., 2013). However, *Cebpa* is expressed at very low levels in T lineage progenitors, and *Lmo2* is turned off before the DN2a stage, well before *Spi1* levels start going down (Hosokawa and Rothenberg, 2021; Yui and Rothenberg, 2014; Zhou et al., 2019). Thus, these indirect mechanisms may contribute to, but not fully explain, the stage specificity.

Mutation of the potential repression element enabled *Spi1* to begin expression in a nonexpressing pro–T cell line, under conditions where deletions of other elements suspected to mediate repression had much less effect. Most notably, Cas9 targeting of the three Runx and one GATA motifs in the +3.7-kb element also enabled primary pro–T cells to sustain readily measurable *Spi1* expression in a developmental stage where controls had virtually extinguished it. Thus, the integrity of this element was important for full developmental stage-specific repression. However, it was atypical of elements normally sought through genomic methods. The binding of Runx1 and GATA3, though reproducible under the conditions used, was very weak. This could reflect the ATAC-inaccessible chromatin state at this site both before and after commitment. While the potential silencer region was not conserved among mammals, this region was perfectly overlapped by a LINE element. LINE elements are known to acquire roles in species-specific gene expression via activation and repression of proximal genes (Robbez-Masson and Rowe, 2015). Furthermore, a recent report on 3D structure of the human *SPI1* locus in monocytes suggest interactions of the promoter with the intron 2 region of *SPI1* as well as with the URE (Schuetzmann et al., 2018). Hence, stage-specific repression of human *SPI1* could be regulated in part via similar or independent human-specific elements, even though the *SPI1* locus overall has multiple conserved cis-regulatory elements.

In summary, we identified a potential stage-specific silencer region for *Spi1*, which appears to be controlled by Runx1 and GATA3, in early T cell development. Acute deletion of *Runx1* and *Gata3* by CRISPR-Cas9 revealed stage-specific roles of Runx1 and GATA3 in *Spi1* repression in pro–T cell stages. A postcommitment stage-specific Runx1 and GATA3 occupancy site at the *Spi1* locus was elucidated by comparative ChIP-seq analysis using precommitment and postcommitment pro–T cells, in the same T lineage pathway but with a few days difference on the trajectory. Acute deletion evidence then supported a strong role for this site in physiological *Spi1* repression. Thus, the developmentally based strategy used in this study could be useful to identify other functionally important cis-regulatory elements, whether or not they were in open chromatin or phylogenetically conserved.

Materials and methods

Mice

C57BL/6 (referred to as B6), B6.Cg-Tg(BCL2)25Wehi/J (Bcl2-Tg; Strasser et al., 1991), and B6.Gt(ROSA)26$^{Sortm1.1(CAG-cas9*,-EGFP)Fezh}$/J (Cas9; Platt et al., 2014) mice were purchased from The Jackson Laboratory. Bcl11b-YFP (backcrossed to C57BL/6 mice 10 times) mice were described previously (Ng et al., 2018). All animals were bred and maintained in the California Institute of Technology Laboratory Animal Facility under specific pathogen–free conditions, and the protocol supporting animal breeding for this work was reviewed and approved by the Institute Animal Care and Use Committee of the California Institute of Technology.

Cell culture of primary pro–T cells

For in vitro differentiation of pro–T cells, BM hematopoietic progenitors were used for input to OP9-DLL1 co-cultures (Schmitt and Zúñiga-Pflücker, 2002). In the conditions used, most cells underwent commitment around days 6–7 of culture.

Vectors carrying genes for gain of function assays or CRISPR guide RNAs for knockout assays were introduced at different time points, depending on whether the cells were to be targeted before, after, or during commitment. Cells for gain-of-function experiments were harvested 3 d after transduction, and cells for loss-of-function experiments were harvested 4 d after transduction in most cases. The *Bcl2* transgene (Tg) was present in the input cells for all these manipulations because it enhances viable recovery of cells under regulatory perturbations, allowing the RNA and protein expression to be measured in a more representative fraction of the responding cells, without altering early T cell development of controls (Yui et al., 2010).

BM was removed from the femurs and tibiae of 2–3-mo-old mice. Suspensions of BM cells were prepared and stained for lineage-specific, mature-cell markers (Lin) using the biotin-conjugated lineage antibodies CD11b (eBioscience; 13–0112-86), CD11c (13–0114-85), Gr-1 (13–5931-86), TER-119 (13–5921-85), NK1.1 (13–5941-85), CD19 (13–0193-85), and CD3ε (13–0031-082). They were then incubated with streptavidin-coated magnetic beads (Miltenyi Biotec) and passed through a magnetic column (Miltenyi Biotec) to remove the Lin^+ cells. Then, the resulting enriched hematopoietic progenitors were cultured on OP9-DLL1 monolayers using OP9 medium (α-MEM, 20% FBS, 50 µM β-mercaptoethanol, and penicillin-streptomycin-glutamine) supplemented with 10 ng/ml IL-7 (Pepro Tech) and 10 ng/ml Flt3L (Pepro Tech). On day 7, cultured cells were disaggregated, filtered through 40-µm nylon mesh, and recultured on new OP9 monolayers with medium containing 5 ng/ml IL-7 and 5 ng/ml Flt3L. In cultures that were continued for longer times, cells were passaged onto fresh OP9-DLL1 monolayers at day 10 and maintained up to day 14 in 1 ng/ml each of IL-7 and Flt3L.

While the developmental trajectory of the cells in these cultures is extremely reproducible between experiments and experimenters, the exact degrees of progression of the cells along the pathway at a given time point often vary slightly from experiment to experiment. For precise measurements of fold change, to establish biological reproducibility with minimum confounding effects of timing on the expression of highly dynamic genes, biological replicate cell samples were prepared separately from three independent animals, purified separately, vector transduced separately, and cultured separately, but in parallel over the same absolute time course. Additional supporting information was obtained in independent experiments.

Cell culture of a pro–T cell-like line

Scid.adh.2c2 cells (Dionne et al., 2005) were cultured in RPMI1640 with 10% FBS (Sigma-Aldrich), sodium pyruvate (Gibco), nonessential amino acids (Gibco), penicillin-streptomycin-glutamine (Gibco), and 50 µM β-mercaptoethanol (Sigma-Aldrich).

Transduction of *Runx1* and *Gata3* into pro–T cells

Gain-of-function experiments were performed before commitment using protocol A (Fig. 2 A). BM progenitor cells from Bcl2-Tg animals were used to seed in vitro differentiation cultures as above. At day 3, the cells were transduced with retroviral vectors encoding reporters (GFP and hNGFR) and the indicated cDNAs (details of vector construction below) and then returned to OP9-DLL1 culture for harvest on day 6 overall. A modification of this protocol was used for gain of function of Runx1 and GATA3 coupled with disruption of the +3.7-kb site motifs as detailed in Fig. 7 A (protocol E). Conditions for Cas9-mediated disruption are described in the next section. The methods used to generate the virus supernatant and for infection were described previously (Hosokawa et al., 2018a). For RT-qPCR analysis, retrovirus-infected $Lin^-CD45^+CD44^+GFP^+hNGFR^+$ (precommitment) cells were sorted on a BD FACSAria.

CRISPR-Cas9–mediated acute deletion of target genes in primary cells and a cell line

Acute deletions of *Gata3* or *Runx1* or their presumptive target sites in primary cells were performed using protocols B, C (Fig. 3, A and D), D, or E (Figs. 6 D and 7 A) to induce deletion in postcommitment, mid-commitment, or precommitment stages, respectively. To generate input cells, Cas9 mice were first bred to Bcl2-Tg mice to generate heterozygotes for both transgenes. BM cells from these Cas9;Bcl2-Tg animals were then used to seed in vitro differentiation cultures as above. At day 10 (for postcommitment effects, protocol B), day 4 (for mid-commitment effects, protocol C), or day 2 (for precommitment effects, protocol D), the cells were transduced with retroviral vectors encoding reporters (GFP, CFP and hNGFR) and the indicated cDNAs or guide RNAs (sgRNAs) as detailed below, and then returned to OP9-DLL1 culture for harvest 4 d later, at day 14 overall (protocol B), day 8 overall (protocol C), or day 6 overall (half of the cultures in protocol D). The other half of the cultures treated early, via protocol D, were continued to day 12 overall to monitor postcommitment effects of precommitment deletion. The methods used to generate the virus supernatant and for infection were as described previously (Hosokawa et al., 2018a). For RT-qPCR analysis, retrovirus-infected Lin^- $CD45^+$ $CD44^+$ GFP^+ $hNGFR^+$ (precommitment) or Lin^- $CD45^+$ $CD44^{lo}$ CFP^+ $hNGFR^+$ (postcommitment) cells were sorted on a BD FACSAria.

A DN3-like cell line, Scid.adh.2c2, previously transduced to express Cas9-GFP, was infected with sgRNA-hNGFR and/or sgRNA-CFP vectors (Hosokawa et al., 2018b). 3 d after sgRNA transduction, sgRNA-introduced $GFP^+CFP^+hNGFR^+$ Scid.adh.2c2 cells were sorted, followed by immunoblotting, or subjected to single-cell sorting. Cytoplasmic and nuclear extracts, used to the detection of tubulinα, and Runx1 and GATA3, respectively, were prepared using NE-PER nuclear and cytoplasmic extraction reagents (Pierce). Lysates were run on 10% polyacrylamide gel, followed by immunoblotting. The antibodies used for the immunoblot analysis were anti-tubulinα (Sigma-Aldrich; T6199), anti-Runx1 (Abcam), anti-Myc (MBL; My3), and anti-GATA3 (Santa Cruz Biotechnology; HG3-31) mAbs.

Cloning

cDNAs for GATA3 WT and mutants were inserted into a multicloning site of the pMxs-IRES-hNGFR, as previously reported (Hosokawa et al., 2015; Hosokawa et al., 2016).

GATA3 residues S308, T315 and S316, which are important for histone deacetylase 2 association in their nonphosphorylated state, are near the C-terminal zinc finger (Hosokawa et al., 2016;

Hosokawa et al., 2013b). GATA3 R261, where arginine methylation increases transcriptional activation potency, is near the N-terminal zinc finger.

cDNA for full-length Runx1 from the distal promoter and Runx1DN (Runx1 d190) were inserted into a multicloning site of the MSCV-IRES-GFP (Telfer et al., 2004). For CRISPR targeting, the sgRNA-expression vector (E42-dTet; Hosokawa et al., 2018b) was used as described previously. For double-KO experiments, versions of E42-dTet with truncated NGFR reporter were made as well the original vector with a CFP reporter (here, mTurquoise2) so that doubly transduced cells could be sorted unambiguously. For site disruption experiments, vectors for sgRNA against Runx motifs were made with an hNGFR reporter, whereas vectors for sgRNA against the GATA motif were made with a CFP reporter. 19- or 20-mer sgRNAs were designed using the CHOPCHOP (https://chopchop.cbu.uib.no; Labun et al., 2016) or Benchling (https://benchling.com) web tool and inserted into the empty sgRNA-expression vector by PCR-based insertion. Three sgRNA-expression vectors were generated for one gene, and pooled retroviral plasmids were used to make retroviral supernatant. The following sgRNA sequences were used in this study: control (Luciferase), 5′-GGCATTTCGCAGCCTACCG-3′; GATA3 #1, 5′-GAGATCCGTGCAGCAGAGG-3′; GATA3 #2, 5′-GTTCCAGGGCGAGGCGGTG-3′; GATA3 #3, 5′-TGGCCGGCCGCCAGAGAAG-3′; Runx1 #1, 5′-GCTCGTGCTGGCATCTACG-3′; Runx1 #2, 5′-AGCCCCGGCAAGATGAGCG-3′; Runx1 #3, 5′-AGCGGCGACCGCAGCATGG-3′; Slc39a13 pro. #1, 5′-GCAGATGCAGCGCTCCGGG-3′; Slc39a13 pro. #2, 5′-AGGGTTACAGTCCTGGAGA-3′; URE #1, 5′-CAAATGGCCCGAGGTCCGA-3′; URE #2, 5′-TACGATCTAGACAGTGGGT-3′; CE4 #1, 5′-TAGAGCTGAGCCTAAGTTC-3′; CE4 #2, 5′-CTGAGGAAGACTTCCAGGT-3′; Spi1 intron2 #1, 5′-CCTGTAATCCTCTCTCGGG-3′; Spi1 intron2 #2, 5′-CACGTGGACCAGAGGTCAC-3′; +145 kb #1, 5′-GGTGTAAGAAGCAGAGTCTG-3′; +145 kb #2, 5′-TTTGTTCACACTGGAAACTG-3′; +167 kb #1, 5′-GCCTACAGCCAGTGGTCGAG-3′; +167 #2, 5′-GGTACGGGTCCTGACGCCGG-3′; +211 #1, 5′-AGAAAGATTCCAATTCAACA-3′; +211 #2, 5′-TCTACTAGGTCTTACCAACT-3′; Runx motif 1, 5′-GATGAACTCAGTGTGGTTT-3′; Runx motif 2, 5′-CTCGACCTGCCCTTAAATG-3′; Runx motif 3, 5′-AAACTAATCTTTTCTCTGT-3′; and GATA motif, 5′-CTCTGTGGGTGCTTATCAC-3′.

Two-step affinity purification of GATA3 complexes from Scid.adh.2c2 cells

Scid.adh.2c2 cells were infected with either mock control (pMxs-IRES-GFP) or Myc-Flag-GATA3–containing retrovirus. 3 dpi, Myc-Flag–tagged GATA3-infected GFP$^+$ cells were solubilized with the following protease inhibitor–containing immunoprecipitation buffer: 50 mM Tris-HCl (pH 7.5), 150 mM NaCl, 10% glycerol, 0.1% Tween, 1 mM EDTA, 10 mM NaF, 1 mM DTT, and a protease inhibitor cocktail (Roche Applied Science) and lysed on ice for 30 min with gentle shaking and sonicated on a Misonix S-4000 sonicator (Qsonica) for three cycles, amplitude 20 for 30 s, followed by a 30-s rest. The insoluble materials were removed by centrifugation, and immunoprecipitation with anti-Flag M2 agarose (Sigma-Aldrich) was performed overnight at 4°C. Immune complexes were eluted from the agarose by 3xFlag peptide (Sigma-Aldrich), and the eluted GATA3 complexes were subjected to a second immunoprecipitation with anti-Myc gel (MBL). Immune complexes were eluted from the gel with Myc peptide (MBL) and separated by SDS-PAGE. The bands were excised from the gel and subjected to a mass spectrometric analysis to identify corresponding proteins. The gel pieces were washed twice with 100 mM bicarbonate in acetonitrile, and the proteins were digested with trypsin. After adding 0.1% formic acid to the supernatant, the peptides were analyzed by liquid chromatography-tandem mass spectrometry with an Advance ultra-high-performance liquid chromatograph (Bruker) and an Orbitrap Velos Pro mass spectrometer (Thermo Fisher Scientific). The resulting tandem mass spectrometry dataset was analyzed using the Mascot software program (Matrix Science). Mascot score is the probability that the observed match is a random event (Mascot score >100 means the absolute probability <1e-10).

Flow cytometry analysis

Thymocytes were isolated from 4–6-wk-old Bcl11b-YFP reporter mice. Lin$^+$ cells were depleted by staining with biotinylated antibodies against CD8α (eBioscience; 13–0081-86), TCRγδ (13–5711-85), TCRβ (13–5961-85), TER-119, NK1.1, Dx5 (13–5971-82), CD11c, and CD11b, then incubating cells with streptavidin magnetic beads, followed by passing them through an LS magnetic column (Miltenyi Biotec) in accordance with the manufacturer's instructions. Purified DN cells were stained with c-Kit APCe780 (eBioscience; 17–1171-82), CD25 PE (12–0251-28), CD44 e450 (48–0441-82), and streptavidin PerCPCy5.5 (45–4317-80) and then subjected to intracellular staining for GATA3 AF647 (BD PharMingen; 560068) or PU.1 AF647 (Cell Signaling; 2240) using the BrdU Flow Kit (BD PharMingen).

For staining of sgRNA-introduced BM cells, surface antibodies against CD45 PECy7 (eBioscience; 25–0451-82), c-Kit APC, CD25 APC-e780 (47–0251-82), human-NGFR PE (12–9400-42), and a biotin-conjugated lineage cocktail (CD8α, CD11b, CD11c, Gr-1, TER-119, NK1.1, CD19, TCRβ, and TCRγδ) with streptavidin PerCPCy5.5 were used for staining.

Prior to cell surface staining, cells were treated with 2.4G2 cell supernatant. All of the cells were analyzed using flow cytometers, MacsQuant 10 (Miltenyi Biotec), LSRFortessa (BD PharMingen), or FACSAria (BD PharMingen) with FlowJo software (Tree Star).

ChIP library construction and characteristics

ChIP experiments and library preparation were performed as previously described (Hosokawa et al., 2018b; Ungerbäck et al., 2018). Briefly, 5–10 × 10^6 cells were fixed with 1 mg/ml DSG (Thermo Fisher Scientific) in PBS for 30 min at room temperature followed by an additional 10 min with addition of formaldehyde up to 1%. These conditions were previously found to give efficient detection of Runx1 binding with strong enrichment for Runx target motifs (Hosokawa et al., 2020; Hosokawa et al., 2018b). 5 µg anti-GATA3 mAbs (a mixture of 2.5 µg sc-268 [Santa Cruz Biotechnology] and 2.5 µg MAB26051 [R&D Systems]) or anti-Runx1 mAb (Abcam; ab23980) was prebound to Dynabeads anti-Mouse or anti-Rabbit Ig (Invitrogen) and then

added to the diluted chromatin complexes. Precipitated chromatin fragments were cleaned up using Zymo ChIP DNA Clean & Concentrator and used as input for qPCR and/or ChIP-seq.

Note that GATA3 shows highly conditional genomic binding patterns at different stages within the T cell lineage, suggesting influence from factors other than its binding affinities for different genomic sequences (Wei et al., 2011; Zhang et al., 2012). For comparison in Fig. S3 A, a separate pair of DN2b/DN3 samples was also prepared for GATA3 ChIP-seq using fixation with 1% formaldehyde only for 10 min, as described previously (Ungerbäck et al., 2018). The patterns of GATA3 occupancy detected depended on the fixation used. GATA3 associations with many enhancer-like sites near suspected positive target genes were consistent, but GATA3 association with closed regions, promoters, and repeat sequence elements appeared systematically different between the two fixation conditions (compare with Fig. S3 A), with characteristics summarized in Fig. S5 F. Briefly, DSG+FA showed higher association with promoters and ATAC-open sites, whereas FA alone showed higher enrichment for strong GATA binding motifs but a substantially higher proportion of binding to repeat sequences. Thus, different fixation conditions could selectively stabilize interactions with different binding-modulatory chromatin contexts. Admixtures of functional sites with different "background" sequences are expected to alter relative enrichment, a key consideration for global statistical comparisons. However, in this study, the goal was maximal absolute recovery of candidates for functionally important sites within the *Spi1* genomic neighborhood to maximize the chance for relevant repression sites to be detected.

Quantitative ChIP-PCR and ChIP-seq

For qPCR analysis, 7900HT Fast Real-time PCR System, QuantStudio3 (Applied Biosystems) or StepOnePlus systems (Applied Biosystems) were used with SYBR GreenER qPCR SuperMix (Invitrogen). The data are shown as the mean values (percent input). Primers are listed below. For deep-sequencing analysis, ChIP-seq libraries were constructed using NEBNext ChIP-Seq Library Preparation Kit (E6240, NEB) and sequenced on Illumina HiSeq2500 in single read mode with the read length of 50 nt. All analyses are based on results from two biologically separate replicates. ChIP-seq data were analyzed as described previously (Hosokawa et al., 2018b; Ungerbäck et al., 2018). BigWigs were generated from the aligned SAM or BED-file formats using Samtools (Li et al., 2009), Bedtools (Quinlan and Hall, 2010) and the UCSC genomeCoverageBed and bedGraphToBigWig and normalized to 1 million reads. For visualization of ChIP-seq tracks, bamToBed and genomeCoverageBed were used with the "-split" setting enabled. BigWig files were up-loaded to the UCSC genome browser (http://genome.ucsc.edu; Speir et al., 2016). Runx1 ChIP-seq data in DN1 and DN2b/3 cells and Runx1 and GATA3 ChIP-seq data in Scid.adh.2c2 cells used in this study were previously published (GEO accession numbers GSE103953 and GSE93755; Hosokawa et al., 2018b): Slc39a13 pro. forward (FW), 5′-CCTTCTGAGGATGCAGTTCC-3′; Slc39a13 pro. reverse (RV), 5′-CTGCTGACTCAGAGAGCCATAG-3′; URE FW, 5′-GGGCGCTTCCTGTTTTCT-3′; URE RV, 5′-CTGGGCAGGGTC AGAGTG-3′; CE4 FW, 5′-TTTGAGGTGCAGGAGACTGA-3′; CE4 RV, 5′-TGAATCTTACTGAACCCCGTCT-3′; intron 2 FW, 5′-CTC GACCTGCCCTTAAATGT-3′; and intron 2 RV, 5′-CCAGTGATA AGCACCCACAG-3′.

qPCR

Total RNA was isolated from samples of 2 × 10^5 cultured cells using a RNeasy Micro Kit (Qiagen). Reverse transcription was performed using the Superscript III kit (Invitrogen). Genomic DNA was isolated from 5 × 10^5 cultured cells using a NucleoSpin Tissue kit (Macherey-Nagel). For qPCR, the 7900HT Fast Real-time PCR System, QuantStudio3 (Applied Biosystems), or StepOnePlus system (Applied Biosystems) were used with SYBR GreenER qPCR SuperMix (Invitrogen). The data are shown as the relative expression normalized to *Actb* (for cDNA) or *Gapdh* promoter (genomic DNA) signals. The following primers were used in this study: PU.1 FW, 5′-TTCTGCACGGGGAGACAG-3′; PU.1 RV, 5′-GTCCACCCACCAGATGCT-3′; GATA3 FW, 5′-TAT CCTCCGACCCACCAC-3′; GATA3 RV, 5′-AAGGGGCTGAGGTTC CAG-3′; Runx1 FW, 5′-CTCCGTGCTACCCACTCACT-3′; Runx1 RV, 5′-ATGACGGTGACCAGAGTGC-3′; Actb FW, TACAGCCCG GGGAGCAT-3′; Actb RV, 5′-ACACCCGCCACCAGTTC-3′; Bcl11b FW, 5′-TGGATGCCAGTGTGAGTTGT-3′; Bcl11b RV, 5′-GCTGCT TGCATGTTGTGC-3′; Slc39a13 pro. FW, 5′-CCTTCTGAGGATGCA GTTCC-3′; Slc39a13 pro. RV, 5′-CTGCTGACTCAGAGAGCCATA G-3′; URE FW, 5′-GGGCGCTTCCTGTTTTCT-3′; URE RV, CTG GGCAGGGTCAGAGTG-3′; CE4 FW, 5′-TTTGAGGTGCAGGAG ACTGA-3′; 5′-CE4 RV, TGAATCTTACTGAACCCCGTCT-3′; intron 2 FW, 5′-CTCGACCTGCCCTTAAATGT-3′; intron 2 RV, 5′-CCAGTGATAAGCACCCACAG-3′; +145 kb FW, 5′-GGCACCTTT AACCCAGAGTTC-3′; +145 kb RV, 5′-AATGAATGACATCAGGCT ACCA-3′; +167 kb FW, 5′-GAAGTTTGGGCCAGTCCAC-3′; +167 kb RV, 5′-TCTGGGCCAATGAACGTC-3′; +211 kb FW, 5′-CTGTAA ACAGGAAACACTCAGCTC-3′; +211 kb RV, 5′-GTGGATGGCTTG CAGTAGG-3′; Ddb2 FW, 5′-TTGGCATCAAGGACAAACCT-3′; Ddb2 RV, 5′-AAACTGGTTGGTATTGAGATGGTT-3′; Pacsin3 FW, 5′-GAAGGCAGACAGCTCCATGT-3′; and Pacsin3 RV, 5′-GGGTCT GCTCATACTGGGTTT-3′.

Statistical analysis

The statistical significance of differences between datasets was determined by two-sided Student's *t* test using Excel. Statistical details of experiments can be found in the figure legends. In all figures, error bars indicate SD.

Online supplemental material

Fig. S1 shows gating strategies for DN subsets in thymocytes and in vitro–differentiated pro–T cells, *Spi1* expression levels in Bcl11b introduced pro–T cells, the ratio of sense and antisense *Spi1* transcripts, proteomics data for GATA3-interacting molecules, and interactions between Runx1 and GATA3 mutants. Fig. S2 shows evidence for successful Runx1 and GATA3 disruption by Cas9 and gating strategies for DN subsets from in vitro–differentiated pro–T cells. Fig. S3 shows a comparison of GATA3 binding sites in different fixation conditions, a comparison of chromatin looping before and after T lineage commitment around the *Spi1* locus, and a comparison of Runx1 and GATA3 binding patterns in phase 1, phase 2, and a DN3-like cell line. Fig.

S4 shows a comparison of Runx1 and GATA3 binding patterns in GATA3- or Runx1-deficient pro–T cells around the *Spi1* locus, Runx1 and GATA3 binding patterns around the postcommitment stage-specific distal chromatin looping sites, and *Spi1* expression levels in +145, +167, or +211 kb element–disrupted DN3-like cell lines. Fig. S5 shows representative consensus motifs for Runx1 and GATA3, gating strategies for DN subsets in BM-derived pro–T cells with motif disruptions, validation of mutations in sg4 motifs mix-transduced pro–T cells, *Spi1* expression levels in the cis-regulatory element disrupted cells, and a table comparing GATA3 occupancy site characteristics under different fixation conditions. Table S1 lists GATA3-interacting molecules in a pro–T cell-like cell line, Scid.adh.2c2.

Data availability

The GEO accession number for all new deep-sequencing data reported in this paper is GSE159960.

Acknowledgments

We thank D. Perez, J. Tijerina, P. Cannon, and R. Diamond for cell sorting and advice, I. Soto for mouse colony care, H. Amrhein and D. Trout for computational assistance, I. Antoshechkin for sequencing management, members of the Support Center for Medical Research and Education at Tokai University for their technical help, and the members of the Rothenberg group for valuable discussion and reagents.

E.V. Rothenberg was supported by the U.S. Public Health Service (grants R01 AI135200, R01AI083514, and R01HD076915). H. Hosokawa was supported by the Japan Society for the Promotion of Science KAKENHI grant JP19H03692, the Uehara Memorial Foundation, the Naito Foundation, the Takeda Science Foundation, the Yasuda Memorial Medical Foundation, the SENSHIN Medical Research Foundation, the Daiichi Sankyo Foundation of Life Science, the Tokyo Biochemical Research Foundation, a Princess Takamatsu Cancer Research Fund research grant, and the 2020 Tokai University School of Medicine Research Aid. T. Tanaka was supported by Japan Society for the Promotion of Science KAKENHI grant JP19H03708, the Uehara Memorial Foundation, the Naito Foundation, the Takeda Science Foundation, the Yasuda Memorial Medical Foundation, the SENSHIN Medical Research Foundation, the NOVARTIS Foundation (Japan) for the Promotion of Science, a Princess Takamatsu Cancer Research Fund research grant, the KOSE Cosmetology Research Foundation, and the Medical Institute of Bioregulation Kyushu University Cooperative Research Project Program. This work was also partly supported by the Tokai University General Research Organization Research and Study Project (H. Hosokawa), the L.A. Garfinkle Memorial Laboratory Fund and the Al Sherman Foundation, Provost and Division of Biology & Biological Engineering of Caltech special project funds, and the Albert Billings Ruddock Professorship (E.V. Rothenberg).

Author contributions: H. Hosokawa designed and supervised the study, performed experiments, analyzed data, and wrote the manuscript; M. Koizumi, K. Masuhara, and M. Romero-Wolf performed experiments and analyzed data; T. Tanaka performed experiments, analyzed data, and edited the manuscript; T. Nakayama provided unique biological reagents and helpful discussions and edited the manuscript; E.V. Rothenberg designed and supervised the study, analyzed data, and wrote the manuscript.

Disclosures: E.V. Rothenberg reported personal fees from Century Therapeutics and personal fees from Kite Pharma outside the submitted work. No other disclosures were reported.

Submitted: 11 December 2020
Revised: 1 May 2021
Accepted: 10 June 2021

References

Boehm, T., L. Foroni, Y. Kaneko, M.F. Perutz, and T.H. Rabbitts. 1991. The rhombotin family of cysteine-rich LIM-domain oncogenes: distinct members are involved in T-cell translocations to human chromosomes 11p15 and 11p13. *Proc. Natl. Acad. Sci. USA.* 88:4367–4371. https://doi.org/10.1073/pnas.88.10.4367

Carotta, S., L. Wu, and S.L. Nutt. 2010. Surprising new roles for PU.1 in the adaptive immune response. *Immunol. Rev.* 238:63–75. https://doi.org/10.1111/j.1600-065X.2010.00955.x

Champhekar, A., S.S. Damle, G. Freedman, S. Carotta, S.L. Nutt, and E.V. Rothenberg. 2015. Regulation of early T-lineage gene expression and developmental progression by the progenitor cell transcription factor PU.1. *Genes Dev.* 29:832–848. https://doi.org/10.1101/gad.259879.115

Chou, S.T., E. Khandros, L.C. Bailey, K.E. Nichols, C.R. Vakoc, Y. Yao, Z. Huang, J.D. Crispino, R.C. Hardison, G.A. Blobel, and M.J. Weiss. 2009. Graded repression of *PU.1/Sfpi1* gene transcription by GATA factors regulates hematopoietic cell fate. *Blood.* 114:983–994. https://doi.org/10.1182/blood-2009-03-207944

Cleveland, S.M., S. Smith, R. Tripathi, E.M. Mathias, C. Goodings, N. Elliott, D. Peng, W. El-Rifai, D. Yi, X. Chen, et al. 2013. Lmo2 induces hematopoietic stem cell-like features in T-cell progenitor cells prior to leukemia. *Stem Cells.* 31:882–894. https://doi.org/10.1002/stem.1345

Dakic, A., D. Metcalf, L. Di Rago, S. Mifsud, L. Wu, and S.L. Nutt. 2005. PU.1 regulates the commitment of adult hematopoietic progenitors and restricts granulopoiesis. *J. Exp. Med.* 201:1487–1502. https://doi.org/10.1084/jem.20050075

Dionne, C.J., K.Y. Tse, A.H. Weiss, C.B. Franco, D.L. Wiest, M.K. Anderson, and E.V. Rothenberg. 2005. Subversion of T lineage commitment by PU.1 in a clonal cell line system. *Dev. Biol.* 280:448–466. https://doi.org/10.1016/j.ydbio.2005.01.027

Ebralidze, A.K., F.C. Guibal, U. Steidl, P. Zhang, S. Lee, B. Bartholdy, M.A. Jorda, V. Petkova, F. Rosenbauer, G. Huang, et al. 2008. PU.1 expression is modulated by the balance of functional sense and antisense RNAs regulated by a shared cis-regulatory element. *Genes Dev.* 22:2085–2092. https://doi.org/10.1101/gad.1654808

Furusawa, J., K. Moro, Y. Motomura, K. Okamoto, J. Zhu, H. Takayanagi, M. Kubo, and S. Koyasu. 2013. Critical role of p38 and GATA3 in natural helper cell function. *J. Immunol.* 191:1818–1826. https://doi.org/10.4049/jimmunol.1300379

Growney, J.D., H. Shigematsu, Z. Li, B.H. Lee, J. Adelsperger, R. Rowan, D.P. Curley, J.L. Kutok, K. Akashi, I.R. Williams, et al. 2005. Loss of *Runx1* perturbs adult hematopoiesis and is associated with a myeloproliferative phenotype. *Blood.* 106:494–504. https://doi.org/10.1182/blood-2004-08-3280

Guo, Y., I. Maillard, S. Chakraborti, E.V. Rothenberg, and N.A. Speck. 2008. Core binding factors are necessary for natural killer cell development and cooperate with Notch signaling during T-cell specification. *Blood.* 112:480–492. https://doi.org/10.1182/blood-2007-10-120261

Heinz, S., C. Benner, N. Spann, E. Bertolino, Y.C. Lin, P. Laslo, J.X. Cheng, C. Murre, H. Singh, and C.K. Glass. 2010. Simple combinations of lineage-determining transcription factors prime cis-regulatory elements required for macrophage and B cell identities. *Mol. Cell.* 38:576–589. https://doi.org/10.1016/j.molcel.2010.05.004

Heinz, S., C.E. Romanoski, C. Benner, K.A. Allison, M.U. Kaikkonen, L.D. Orozco, and C.K. Glass. 2013. Effect of natural genetic variation on

enhancer selection and function. *Nature.* 503:487–492. https://doi.org/10.1038/nature12615

Homminga, I., R. Pieters, A.W. Langerak, J.J. de Rooi, A. Stubbs, M. Verstegen, M. Vuerhard, J. Buijs-Gladdines, C. Kooi, P. Klous, et al. 2011. Integrated transcript and genome analyses reveal NKX2-1 and MEF2C as potential oncogenes in T cell acute lymphoblastic leukemia. *Cancer Cell.* 19: 484–497. https://doi.org/10.1016/j.ccr.2011.02.008

Hoogenkamp, M., H. Krysinska, R. Ingram, G. Huang, R. Barlow, D. Clarke, A. Ebralidze, P. Zhang, H. Tagoh, P.N. Cockerill, et al. 2007. The *Pu.1* locus is differentially regulated at the level of chromatin structure and noncoding transcription by alternate mechanisms at distinct developmental stages of hematopoiesis. *Mol. Cell. Biol.* 27:7425–7438. https://doi.org/10.1128/MCB.00905-07

Hosokawa, H., and E.V. Rothenberg. 2018. Cytokines, Transcription Factors, and the Initiation of T-Cell Development. *Cold Spring Harb. Perspect. Biol.* 10:a028621. https://doi.org/10.1101/cshperspect.a028621

Hosokawa, H., and E.V. Rothenberg. 2021. How transcription factors drive choice of the T cell fate. *Nat. Rev. Immunol.* 21:162–176. https://doi.org/10.1038/s41577-020-00426-6

Hosokawa, H., T. Tanaka, M. Kato, K. Shinoda, H. Tohyama, A. Hanazawa, Y. Tamaki, K. Hirahara, R. Yagi, I. Sakikawa, et al. 2013a. Gata3/Ruvbl2 complex regulates T helper 2 cell proliferation via repression of Cdkn2c expression. *Proc. Natl. Acad. Sci. USA.* 110:18626–18631. https://doi.org/10.1073/pnas.1311100110

Hosokawa, H., T. Tanaka, Y. Suzuki, C. Iwamura, S. Ohkubo, K. Endoh, M. Kato, Y. Endo, A. Onodera, D.J. Tumes, et al. 2013b. Functionally distinct Gata3/Chd4 complexes coordinately establish T helper 2 (Th2) cell identity. *Proc. Natl. Acad. Sci. USA.* 110:4691–4696. https://doi.org/10.1073/pnas.1220865110

Hosokawa, H., M. Kato, H. Tohyama, Y. Tamaki, Y. Endo, M.Y. Kimura, D.J. Tumes, S. Motohashi, M. Matsumoto, K.I. Nakayama, et al. 2015. Methylation of Gata3 protein at Arg-261 regulates transactivation of the Il5 gene in T helper 2 cells. *J. Biol. Chem.* 290:13095–13103. https://doi.org/10.1074/jbc.M114.621524

Hosokawa, H., T. Tanaka, Y. Endo, M. Kato, K. Shinoda, A. Suzuki, S. Motohashi, M. Matsumoto, K.I. Nakayama, and T. Nakayama. 2016. Akt1-mediated Gata3 phosphorylation controls the repression of IFNγ in memory-type Th2 cells. *Nat. Commun.* 7:11289. https://doi.org/10.1038/ncomms11289

Hosokawa, H., M. Romero-Wolf, M.A. Yui, J. Ungerbäck, M.L.G. Quiloan, M. Matsumoto, K.I. Nakayama, T. Tanaka, and E.V. Rothenberg. 2018a. Bcl11b sets pro–T cell fate by site-specific cofactor recruitment and by repressing *Id2* and *Zbtb16*. *Nat. Immunol.* 19:1427–1440. https://doi.org/10.1038/s41590-018-0238-4

Hosokawa, H., J. Ungerbäck, X. Wang, M. Matsumoto, K.I. Nakayama, S.M. Cohen, T. Tanaka, and E.V. Rothenberg. 2018b. Transcription Factor PU.1 Represses and Activates Gene Expression in Early T Cells by Redirecting Partner Transcription Factor Binding. *Immunity.* 48: 1119–1134.e7. https://doi.org/10.1016/j.immuni.2018.04.024

Hosokawa, H., M. Romero-Wolf, Q. Yang, Y. Motomura, D. Levanon, Y. Groner, K. Moro, T. Tanaka, and E.V. Rothenberg. 2020. Cell type-specific actions of Bcl11b in early T-lineage and group 2 innate lymphoid cells. *J. Exp. Med.* 217:e20190972. https://doi.org/10.1084/jem.20190972

Hosokawa, H., K. Masuhara, and M. Koizumi. 2021. Transcription factors regulate early T cell development via redeployment of other factors: Functional dynamics of constitutively required factors in cell fate decisions. *BioEssays.* 43:e2000345. https://doi.org/10.1002/bies.202000345

Hu, G., K. Cui, D. Fang, S. Hirose, X. Wang, D. Wangsa, W. Jin, T. Ried, P. Liu, J. Zhu, et al. 2018. Transformation of Accessible Chromatin and 3D Nucleome Underlies Lineage Commitment of Early T Cells. *Immunity.* 48:227–242.e8. https://doi.org/10.1016/j.immuni.2018.01.013

Huang, G., P. Zhang, H. Hirai, S. Elf, X. Yan, Z. Chen, S. Koschmieder, Y. Okuno, T. Dayaram, J.D. Growney, et al. 2008. PU.1 is a major downstream target of AML1 (RUNX1) in adult mouse hematopoiesis. *Nat. Genet.* 40:51–60. https://doi.org/10.1038/ng.2007.7

Kueh, H.Y., A. Champhekar, S.L. Nutt, M.B. Elowitz, and E.V. Rothenberg. 2013. Positive feedback between PU.1 and the cell cycle controls myeloid differentiation. *Science.* 341:670–673. https://doi.org/10.1126/science.1240831

Kueh, H.Y., M.A. Yui, K.K. Ng, S.S. Pease, J.A. Zhang, S.S. Damle, G. Freedman, S. Siu, I.D. Bernstein, M.B. Elowitz, and E.V. Rothenberg. 2016. Asynchronous combinatorial action of four regulatory factors activates *Bcl11b* for T cell commitment. *Nat. Immunol.* 17:956–965. https://doi.org/10.1038/ni.3514

Labun, K., T.G. Montague, J.A. Gagnon, S.B. Thyme, and E. Valen. 2016. CHOPCHOP v2: a web tool for the next generation of CRISPR genome engineering. *Nucleic Acids Res.* 44(W1):W272–W276. https://doi.org/10.1093/nar/gkw398

Laiosa, C.V., M. Stadtfeld, H. Xie, L. de Andres-Aguayo, and T. Graf. 2006. Reprogramming of committed T cell progenitors to macrophages and dendritic cells by C/EBP α and PU.1 transcription factors. *Immunity.* 25: 731–744. https://doi.org/10.1016/j.immuni.2006.09.011

Li, Y., Y. Okuno, P. Zhang, H.S. Radomska, H. Chen, H. Iwasaki, K. Akashi, M.J. Klemsz, S.R. McKercher, R.A. Maki, and D.G. Tenen. 2001. Regulation of the PU.1 gene by distal elements. *Blood.* 98:2958–2965. https://doi.org/10.1182/blood.V98.10.2958

Li, H., B. Handsaker, A. Wysoker, T. Fennell, J. Ruan, N. Homer, G. Marth, G. Abecasis, and R. Durbin. 1000 Genome Project Data Processing Subgroup. 2009. The Sequence Alignment/Map format and SAMtools. *Bioinformatics.* 25:2078–2079. https://doi.org/10.1093/bioinformatics/btp352

Longabaugh, W.J.R., W. Zeng, J.A. Zhang, H. Hosokawa, C.S. Jansen, L. Li, M. Romero-Wolf, P. Liu, H.Y. Kueh, A. Mortazavi, and E.V. Rothenberg. 2017. Bcl11b and combinatorial resolution of cell fate in the T-cell gene regulatory network. *Proc. Natl. Acad. Sci. USA.* 114:5800–5807. https://doi.org/10.1073/pnas.1610617114

Lu, M., R. Tayu, T. Ikawa, K. Masuda, I. Matsumoto, H. Mugishima, H. Kawamoto, and Y. Katsura. 2005. The earliest thymic progenitors in adults are restricted to T, NK, and dendritic cell lineage and have a potential to form more diverse TCRβ chains than fetal progenitors. *J. Immunol.* 175:5848–5856. https://doi.org/10.4049/jimmunol.175.9.5848

Montecino-Rodriguez, E., D. Casero, M. Fice, J. Le, and K. Dorshkind. 2018. Differential Expression of PU.1 and Key T Lineage Transcription Factors Distinguishes Fetal and Adult T Cell Development. *J. Immunol.* 200: 2046–2056. https://doi.org/10.4049/jimmunol.1701336

Nakayama, T., K. Hirahara, A. Onodera, Y. Endo, H. Hosokawa, K. Shinoda, D.J. Tumes, and Y. Okamoto. 2017. Th2 Cells in Health and Disease. *Annu. Rev. Immunol.* 35:53–84. https://doi.org/10.1146/annurev-immunol-051116-052350

Ng, K.K.H., M.A. Yui, A. Mehta, S. Siu, B. Irwin, S. Pease, S. Hirose, M.B. Elowitz, E.V. Rothenberg, and H.Y. Kueh. 2018. A stochastic epigenetic switch controls the dynamics of T-cell lineage commitment. *eLife.* 7: e37851. https://doi.org/10.7554/eLife.37851

Okuno, Y., G. Huang, F. Rosenbauer, E.K. Evans, H.S. Radomska, H. Iwasaki, K. Akashi, F. Moreau-Gachelin, Y. Li, P. Zhang, et al. 2005. Potential autoregulation of transcription factor PU.1 by an upstream regulatory element. *Mol. Cell. Biol.* 25:2832–2845. https://doi.org/10.1128/MCB.25.7.2832-2845.2005

Ostuni, R., V. Piccolo, I. Barozzi, S. Polletti, A. Termanini, S. Bonifacio, A. Curina, E. Prosperini, S. Ghisletti, and G. Natoli. 2013. Latent enhancers activated by stimulation in differentiated cells. *Cell.* 152:157–171. https://doi.org/10.1016/j.cell.2012.12.018

Platt, R.J., S. Chen, Y. Zhou, M.J. Yim, L. Swiech, H.R. Kempton, J.E. Dahlman, O. Parnas, T.M. Eisenhaure, M. Jovanovic, et al. 2014. CRISPR-Cas9 knockin mice for genome editing and cancer modeling. *Cell.* 159: 440–455. https://doi.org/10.1016/j.cell.2014.09.014

Quinlan, A.R., and I.M. Hall. 2010. BEDTools: a flexible suite of utilities for comparing genomic features. *Bioinformatics.* 26:841–842. https://doi.org/10.1093/bioinformatics/btq033

Radtke, F., H.R. MacDonald, and F. Tacchini-Cottier. 2013. Regulation of innate and adaptive immunity by Notch. *Nat. Rev. Immunol.* 13:427–437. https://doi.org/10.1038/nri3445

Robbez-Masson, L., and H.M. Rowe. 2015. Retrotransposons shape species-specific embryonic stem cell gene expression. *Retrovirology.* 12:45. https://doi.org/10.1186/s12977-015-0173-5

Romero-Wolf, M., B. Shin, W. Zhou, M. Koizumi, E.V. Rothenberg, and H. Hosokawa. 2020. Notch2 complements Notch1 to mediate inductive signaling that initiates early T cell development. *J. Cell Biol.* 219: e202005093. https://doi.org/10.1083/jcb.202005093

Rosenbauer, F., K. Wagner, J.L. Kutok, H. Iwasaki, M.M. Le Beau, Y. Okuno, K. Akashi, S. Fiering, and D.G. Tenen. 2004. Acute myeloid leukemia induced by graded reduction of a lineage-specific transcription factor, PU.1. *Nat. Genet.* 36:624–630. https://doi.org/10.1038/ng1361

Rosenbauer, F., B.M. Owens, L. Yu, J.R. Tumang, U. Steidl, J.L. Kutok, L.K. Clayton, K. Wagner, M. Scheller, H. Iwasaki, et al. 2006. Lymphoid cell growth and transformation are suppressed by a key regulatory element of the gene encoding PU.1. *Nat. Genet.* 38:27–37. https://doi.org/10.1038/ng1679

Rothenberg, E.V., J.E. Moore, and M.A. Yui. 2008. Launching the T-cell-lineage developmental programme. *Nat. Rev. Immunol.* 8:9–21. https://doi.org/10.1038/nri2232

Rothenberg, E.V., H. Hosokawa, and J. Ungerbäck. 2019. Mechanisms of Action of Hematopoietic Transcription Factor PU.1 in Initiation of T-Cell Development. *Front. Immunol.* 10:228. https://doi.org/10.3389/fimmu.2019.00228

Schmitt, T.M., and J.C. Zúñiga-Pflücker. 2002. Induction of T cell development from hematopoietic progenitor cells by Delta-like-1 in vitro. *Immunity*. 17:749–756. https://doi.org/10.1016/S1074-7613(02)00474-0

Schuetzmann, D., C. Walter, B. van Riel, S. Kruse, T. König, T. Erdmann, A. Tönges, E. Bindels, A. Weilemann, C. Gebhard, et al. 2018. Temporal autoregulation during human PU.1 locus SubTAD formation. *Blood.* 132:2643–2655. https://doi.org/10.1182/blood-2018-02-834721

Scott, E.W., M.C. Simon, J. Anastasi, and H. Singh. 1994. Requirement of transcription factor PU.1 in the development of multiple hematopoietic lineages. *Science*. 265:1573–1577. https://doi.org/10.1126/science.8079170

Scripture-Adams, D.D., S.S. Damle, L. Li, K.J. Elihu, S. Qin, A.M. Arias, R.R. Butler III, A. Champhekar, J.A. Zhang, and E.V. Rothenberg. 2014. GATA-3 dose-dependent checkpoints in early T cell commitment. *J. Immunol.* 193:3470–3491. https://doi.org/10.4049/jimmunol.1301663

Seki, M., S. Kimura, T. Isobe, K. Yoshida, H. Ueno, Y. Nakajima-Takagi, C. Wang, L. Lin, A. Kon, H. Suzuki, et al. 2017. Recurrent SPI1 (PU.1) fusions in high-risk pediatric T cell acute lymphoblastic leukemia. *Nat. Genet.* 49:1274–1281. https://doi.org/10.1038/ng.3900

Shin, B., H. Hosokawa, M. Romero-Wolf, W. Zhou, K. Masuhara, V.R. Tobin, D. Levanon, Y. Groner, and E.V. Rothenberg. 2021. Runx1 and Runx3 drive progenitor to T-lineage transcriptome conversion in mouse T cell commitment via dynamic genomic site switching. *Proc. Natl. Acad. Sci. USA.* 118:e2019655118. https://doi.org/10.1073/pnas.2019655118

Singh, H., R.P. DeKoter, and J.C. Walsh. 1999. PU.1, a shared transcriptional regulator of lymphoid and myeloid cell fates. *Cold Spring Harb. Symp. Quant. Biol.* 64:13–20. https://doi.org/10.1101/sqb.1999.64.13

Speir, M.L., A.S. Zweig, K.R. Rosenbloom, B.J. Raney, B. Paten, P. Nejad, B.T. Lee, K. Learned, D. Karolchik, A.S. Hinrichs, et al. 2016. The UCSC Genome Browser database: 2016 update. *Nucleic Acids Res.* 44(D1):D717–D725. https://doi.org/10.1093/nar/gkv1275

Strasser, A., A.W. Harris, and S. Cory. 1991. *bcl-2* transgene inhibits T cell death and perturbs thymic self-censorship. *Cell.* 67:889–899. https://doi.org/10.1016/0092-8674(91)90362-3

Taghon, T., M.A. Yui, and E.V. Rothenberg. 2007. Mast cell lineage diversion of T lineage precursors by the essential T cell transcription factor GATA-3. *Nat. Immunol.* 8:845–855. https://doi.org/10.1038/ni1486

Telfer, J.C., E.E. Hedblom, M.K. Anderson, M.N. Laurent, and E.V. Rothenberg. 2004. Localization of the domains in Runx transcription factors required for the repression of CD4 in thymocytes. *J. Immunol.* 172:4359–4370. https://doi.org/10.4049/jimmunol.172.7.4359

Ungerbäck, J., H. Hosokawa, X. Wang, T. Strid, B.A. Williams, M. Sigvardsson, and E.V. Rothenberg. 2018. Pioneering, chromatin remodeling, and epigenetic constraint in early T-cell gene regulation by SPI1 (PU.1). *Genome Res.* 28:1508–1519. https://doi.org/10.1101/gr.231423.117

Vangala, R.K., M.S. Heiss-Neumann, J.S. Rangatia, S.M. Singh, C. Schoch, D.G. Tenen, W. Hiddemann, and G. Behre. 2003. The myeloid master regulator transcription factor PU.1 is inactivated by AML1-ETO in t(8;21) myeloid leukemia. *Blood.* 101:270–277. https://doi.org/10.1182/blood-2002-04-1288

Wang, D., J. D'Costa, C.I. Civin, and A.D. Friedman. 2006. C/EBPα directs monocytic commitment of primary myeloid progenitors. *Blood*. 108:1223–1229. https://doi.org/10.1182/blood-2005-12-008763

Wei, G., B.J. Abraham, R. Yagi, R. Jothi, K. Cui, S. Sharma, L. Narlikar, D.L. Northrup, Q. Tang, W.E. Paul, et al. 2011. Genome-wide analyses of transcription factor GATA3-mediated gene regulation in distinct T cell types. *Immunity.* 35:299–311. https://doi.org/10.1016/j.immuni.2011.08.007

Yamagata, T., K. Mitani, H. Oda, T. Suzuki, H. Honda, T. Asai, K. Maki, T. Nakamoto, and H. Hirai. 2000. Acetylation of GATA-3 affects T-cell survival and homing to secondary lymphoid organs. *EMBO J.* 19:4676–4687. https://doi.org/10.1093/emboj/19.17.4676

Yang, Q., J. Jeremiah Bell, and A. Bhandoola. 2010. T-cell lineage determination. *Immunol. Rev.* 238:12–22. https://doi.org/10.1111/j.1600-065X.2010.00956.x

Yeamans, C., D. Wang, I. Paz-Priel, B.E. Torbett, D.G. Tenen, and A.D. Friedman. 2007. C/EBPα binds and activates the PU.1 distal enhancer to induce monocyte lineage commitment. *Blood*. 110:3136–3142. https://doi.org/10.1182/blood-2007-03-080291

Yoshida, H., C.A. Lareau, R.N. Ramirez, S.A. Rose, B. Maier, A. Wroblewska, F. Desland, A. Chudnovskiy, A. Mortha, C. Dominguez, et al. Immunological Genome Project. 2019. The cis-Regulatory Atlas of the Mouse Immune System. *Cell.* 176:897–912.e20. https://doi.org/10.1016/j.cell.2018.12.036

Yui, M.A., and E.V. Rothenberg. 2014. Developmental gene networks: a triathlon on the course to T cell identity. *Nat. Rev. Immunol.* 14:529–545. https://doi.org/10.1038/nri3702

Yui, M.A., N. Feng, and E.V. Rothenberg. 2010. Fine-scale staging of T cell lineage commitment in adult mouse thymus. *J. Immunol.* 185:284–293. https://doi.org/10.4049/jimmunol.1000679

Zarnegar, M.A., J. Chen, and E.V. Rothenberg. 2010. Cell-type-specific activation and repression of PU.1 by a complex of discrete, functionally specialized cis-regulatory elements. *Mol. Cell. Biol.* 30:4922–4939. https://doi.org/10.1128/MCB.00354-10

Zhang, J.A., A. Mortazavi, B.A. Williams, B.J. Wold, and E.V. Rothenberg. 2012. Dynamic transformations of genome-wide epigenetic marking and transcriptional control establish T cell identity. *Cell.* 149:467–482. https://doi.org/10.1016/j.cell.2012.01.056

Zhou, W., M.A. Yui, B.A. Williams, J. Yun, B.J. Wold, L. Cai, and E.V. Rothenberg. 2019. Single-cell analysis reveals regulatory gene expression dynamics leading to lineage commitment in early T cell development. *Cell Syst.* 9:321–337.e9. https://doi.org/10.1016/j.cels.2019.09.008

JEM

Supplemental material

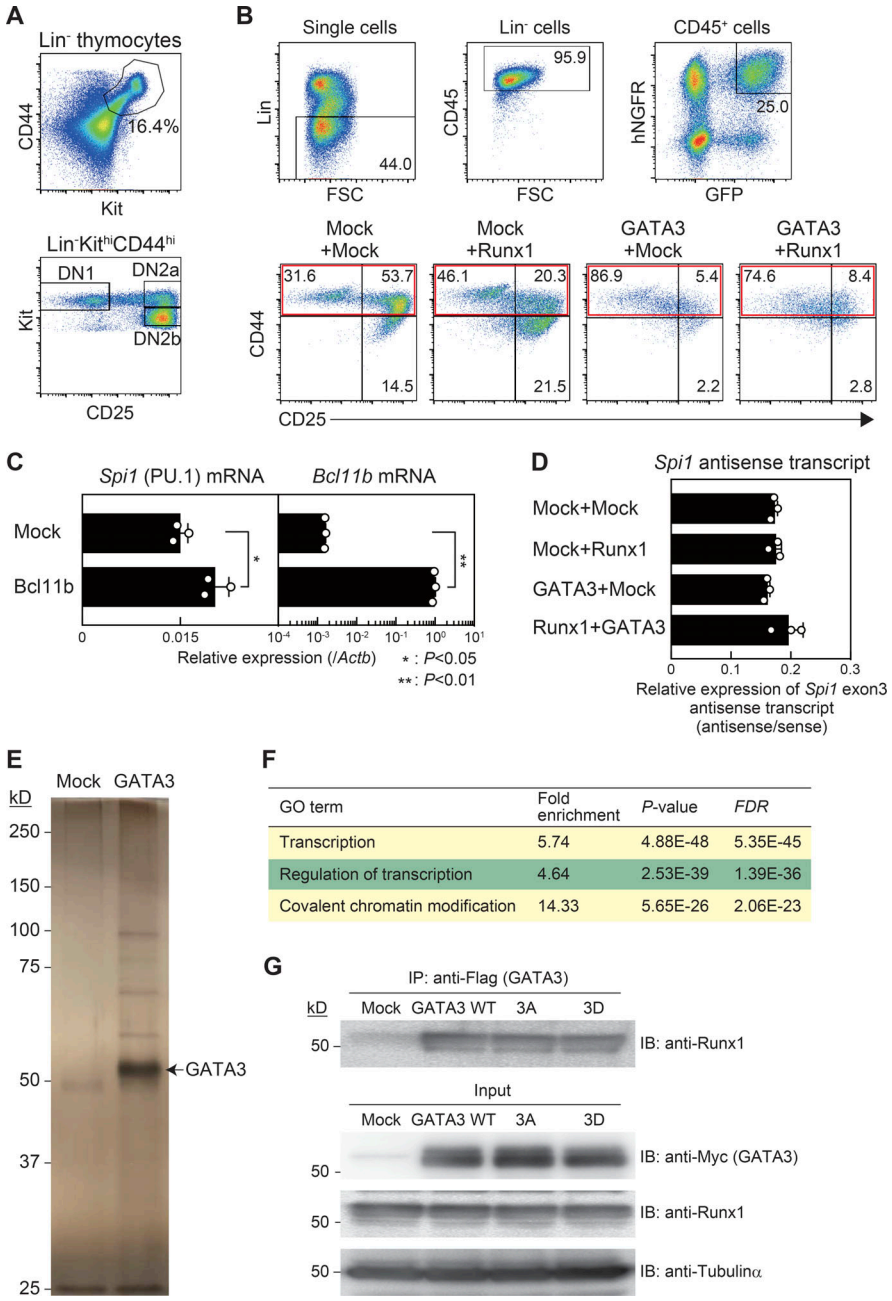

GO term	Fold enrichment	*P*-value	*FDR*
Transcription	5.74	4.88E-48	5.35E-45
Regulation of transcription	4.64	2.53E-39	1.39E-36
Covalent chromatin modification	14.33	5.65E-26	2.06E-23

Figure S1. **Effects of Runx1, GATA3, or Bcl11b introduction on *Spi1* expression in precommitment pro–T stages. (A)** Flow cytometric analysis of thymocytes from Bcl11b-YFP reporter mice was performed. Representative Kit/CD44 profile in Lin⁻ cells (top) and CD25/Kit profile in Lin⁻Kit^{hi}CD44^{hi} cells (bottom) are shown. Results are representative of three independent experiments. **(B)** Flow cytometric analysis of retrovirus-infected Lin⁻CD45⁺CD44⁺GFP⁺hNGFR⁺ precommitment cells was performed at 3 d after introduction using protocol A. Gating strategy for Lin⁻CD45⁺GFP⁺hNGFR⁺ cells is shown (top). Representative profiles of CD44/CD25 in Lin⁻CD45⁺GFP⁺hNGFR⁺ cells are shown (bottom). Gates to isolate CD44⁺ cells for sorting are labeled with red rectangles. Results are representative of three independent experiments. **(C)** Retrovirus encoding *Bcl11b* was infected into precommitment cells, and then Lin⁻CD45⁺CD44⁺GFP⁺hNGFR⁺ cells were sorted at 3 d after introduction from protocol A. Expression levels of *Spi1* and *Bcl11b* were analyzed by RT-qPCR. The relative expression (/*Actb*) is shown with SD. *, P < 0.05; **, P < 0.01 by two-sided Student's *t* test. Data are based on three biological replicates. **(D)** Retrovirus-infected Lin⁻CD45⁺CD44⁺GFP⁺hNGFR⁺ precommitment cells were sorted at 3 d after introduction (protocol A). Strand-specific cDNAs around the exon 3 region of the *Spi1* locus were synthesized as described previously (Ebralidze et al., 2008). Ratio of antisense transcripts against sense transcripts (antisense/sense) of *Spi1* exon3 is shown with SD. Data are based on three biological replicates. **(E)** Myc- and Flag-tagged (double epitope–tagged) GATA3 was retrovirally transduced into a DN3-like cell line, Scid.adh.2c2. Total extracts from Myc-Flag-GATA3–expressing Scid.adh.2c2 cells were subjected to two-step affinity purification followed by SDS-PAGE and silver staining. All of the visible bands were subjected to mass spectrometry analysis. Data are representative of two independent experiments. **(F)** Gene Ontology (GO) annotation of proteins identified from their GATA3-interacting peptides was performed using the DAVID analysis tool (http://david.ncifcrf.gov/). Top three GO terms for GATA3-interacting molecules (Table S1) are shown. **(G)** Total extracts from Scid.adh.2c2 cells transduced with Myc-Flag-GATA3 WT, -3A, or -3D were subjected to immunoprecipitation (IP) with anti-Flag mAb followed by immunoblotting (IB) with anti-Runx1 antibodies. To measure protein levels in the inputs, nuclear or cytoplasmic lysates were subjected to IB with anti-Myc (GATA3), anti-Runx1, or anti-tubulinα antibodies, respectively (input). Data are representative of three independent experiments.

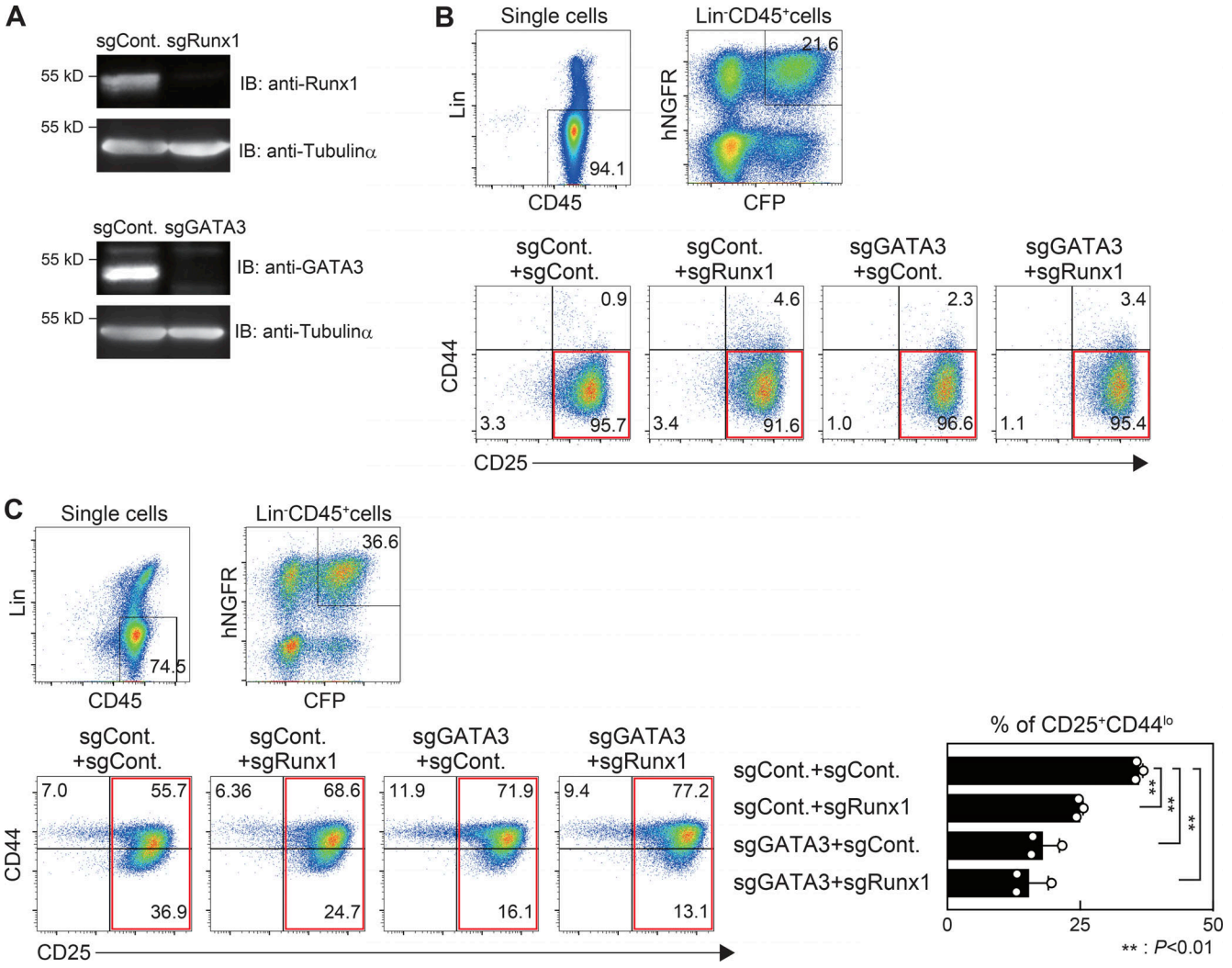

Figure S2. **Effects of Runx1 or GATA3 perturbations on *Spi1* expression in postcommitment pro–T stages. (A)** To test Cas9-mediated disruption, Scid.adh.2c2 cells already expressing Cas9 from a GFP$^+$ vector were transduced with sgRunx1 or control in an hNGFR$^+$ vector or with sgGata3 or control in a CFP$^+$ vector. 3 d after sgRNA transduction, lysates from the retrovirus-infected Cas9-GFP$^+$CFP$^+$ or Cas9-GFP$^+$hNGFR$^+$ Scid.adh.2c2 cells were subjected to immunoblotting (IB) for Runx1 (top) and GATA3 (bottom), respectively. Two independent experiments were performed with similar results. **(B)** Flow cytometric analyses of retrovirus-infected Lin$^-$CD45$^+$CFP$^+$hNGFR$^+$ postcommitment primary cells were performed at 4 d after transduction using protocol B. Gating strategies for Lin$^-$CD45$^+$GFP$^+$hNGFR$^+$ cells are shown (top). Representative profiles of CD44/CD25 in Lin$^-$CD45$^+$GFP$^+$hNGFR$^+$ cells are shown (bottom). Gates to define CD44^{lo} cells for sorting are labeled with red rectangles. Results are representative of three independent experiments. **(C)** Lin$^-$CD45$^+$CFP$^+$hNGFR$^+$ cells that had been transduced with sgRNAs before commitment were subjected to flow cytometric analysis at 4 d after transduction using protocol C. Gating strategies for Lin$^-$CD45$^+$GFP$^+$hNGFR$^+$ cells are shown (top). Representative profiles of CD44/CD25 in Lin$^-$CD45$^+$GFP$^+$hNGFR$^+$ cells are shown (bottom). CD25$^+$ cells for sorting were labeled with red rectangles. The percentages of CD25$^+$CD44^{lo} cells are indicated with SD. **, P < 0.01 by two-sided Student's *t* test for the indicated sample pairs. Data are representative of two independent experiments and based on three biological replicates in an experiment.

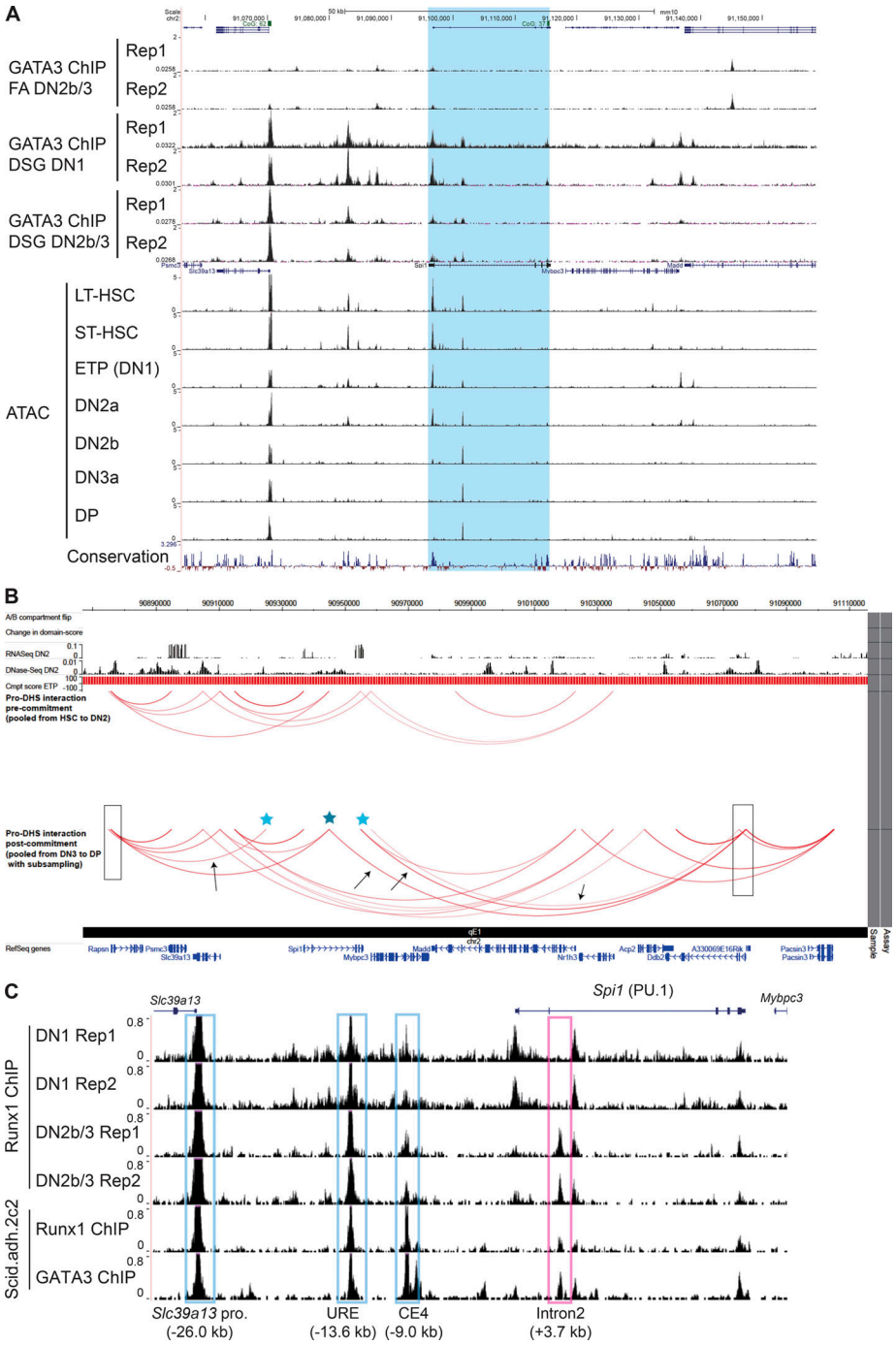

Figure S3. **GATA3 and Runx1 modestly bind to the intronic region of the *Spi1* locus in DN2b/3 and Scid.adh.2c2 cells. (A)** Sensitivity of GATA3 DNA-binding pattern to ChIP-seq cross-linking conditions. FA+DSG-cross-linked DN1 and DN2b/3 cells and FA cross-linked DN2b/3 cells were subjected to ChIP-seq analysis for GATA3. ChIP-seq tracks around the *Spi1* locus are shown with representative ATAC-sequencing tracks in long-term hematopoietic stem cells (LT-HSC), short-term (ST-) HSC, DN1, DN2a, DN2b, DN3, and double-positive (DP) cells (Yoshida et al., 2019) and the conservation track. The *Spi1* locus is highlighted in light blue. **(B)** Changes in higher-order chromatin looping around the *Spi1* locus before and after pro–T cell commitment, from published Hi-C results of (Hu et al., 2018). Map positions are in mm9 coordinates (top) and therefore show some offset from mm10 coordinates in other figure panels. Gene models are at bottom (RefSeq genes). Tracks for A/B compartment flip and change in domain score are empty due to lack of changes in this genomic region. Active transcription units are indicated by "RNASeq DN2" track, and strongly open chromatin is shown by DNase sequencing from DN2 cells in the study. Arc plots pool data from hematopoietic stem cells to DN2 cells as "precommitment" due to the constancy of their patterns, and data from DN3 to double positive as "postcommitment". Arcs shown are those that connect any promoters to any DNase-sensitive region. Data display was downloaded from the Washington University St. Louis epigenome browser (http://epigenomegateway.wustl.edu/browser/?genome=mm9&session=bxT0F5m0YY). New arcs appearing during commitment that involve the *Spi1* locus are indicated by arrows, and their anchor points in the *Spi1* locus or the *Spi1-Slc39a13* intergenic region (site of the URE) are indicated by blue stars. Dark blue star indicates the intron 2 anchor point. **(C)** DN1, DN2b/3, and Scid.adh.2c2 cells were subjected to ChIP-seq analysis for Runx1 and GATA3 (GSE103953 and GSE93755; Hosokawa et al., 2018b). ChIP-seq tracks around the *Spi1* locus are shown. Previously reported cis-regulatory elements and a DN2b/3-specific Runx1 and GATA3 binding site are labeled with blue and magenta rectangles, respectively.

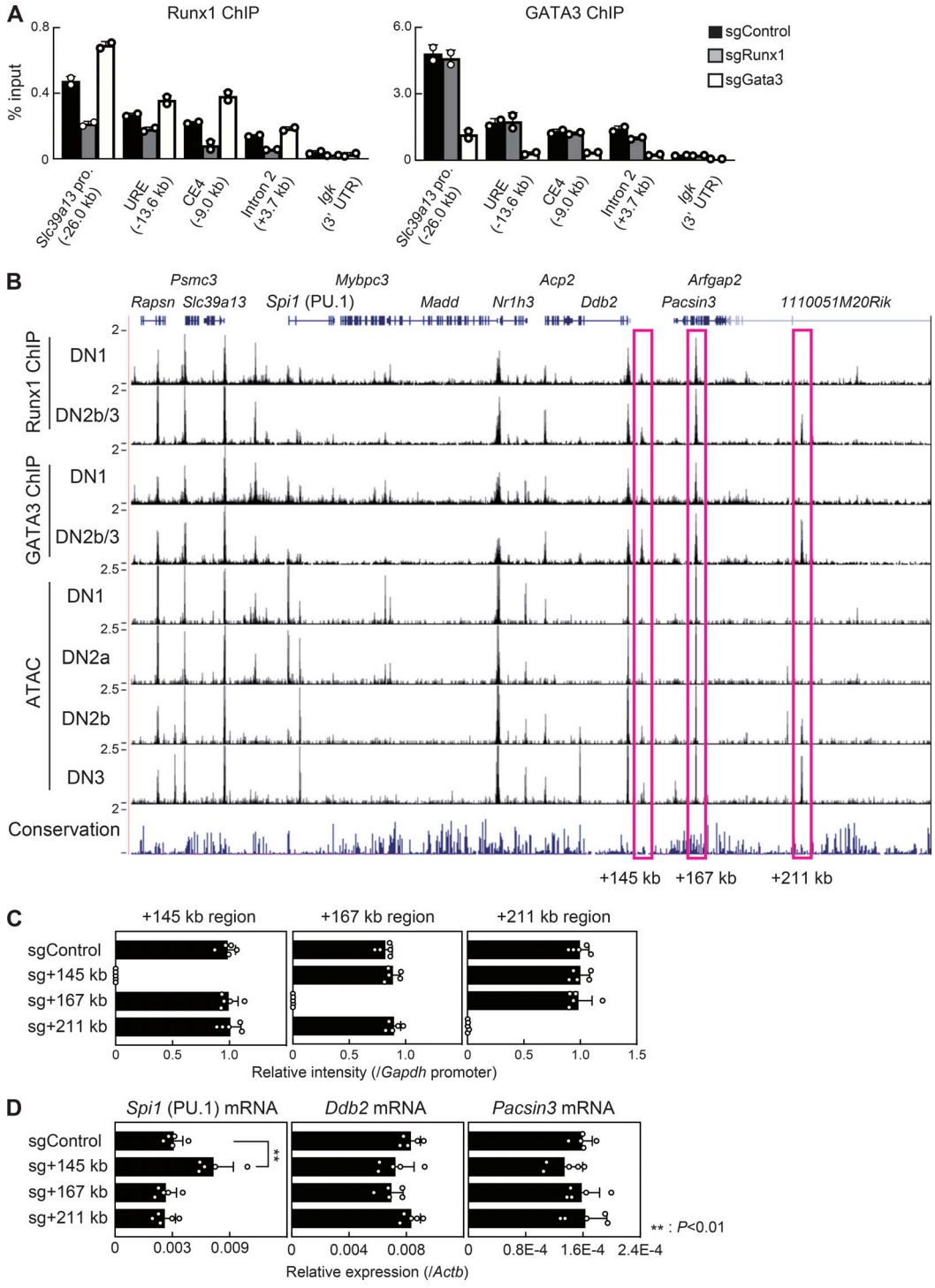

Figure S4. **Potential silencer activity of the DN2b/3-specific looping site around the *Spi1* locus. (A)** Test for interdependence of GATA3 and Runx1 binding to candidate *Spi1* regulatory elements. sgRNA-introduced Lin$^-$CD45$^+$hNGFR$^+$CFP$^+$ postcommitment cells were purified using protocol B, and then the binding of Runx1 and GATA3 at the previously reported cis-regulatory elements and the DN2b/3-specific Runx1 and GATA3 binding site around the *Spi1* locus were determined by ChIP assay with qPCR analysis. The mean values (percent input) are shown with SD. Data are based on two independent experiments. UTR, untranslated region. **(B)** Representative ChIP-seq tracks in DN1 and DN2b/3 cells and ATAC-sequencing tracks in DN1, DN2a, DN2b, and DN3 cells are shown with the conservation track over an extended region around the *Spi1* locus. Runx1 and GATA3 binding sites around the DN2b/3-specific looping site (+145, +167, and +211 kb) are labeled with magenta rectangles. Data are representative of two independent experiments. **(C)** Efficient disruption of candidate distal regulatory elements. Cas9-introduced Scid.adh.2c2 cells were infected with sgRNAs against two sides of the targeted genomic regions (+145-, +167-, and +211-kb sites in B). GFP$^+$CFP$^+$hNGFR$^+$ cells were subjected to single-cell sorting and then expanded for 2 wk, as in Fig. 5 A. Genomic DNA from each clone was isolated and subjected to qPCR analysis to confirm deletion of the targeted genomic regions. The relative intensity (/*Gapdh* promoter) is shown with SD. Data are based on five independent clones from each sgRNA transduction. **(D)** Relative expression levels of *Spi1*, against *Actb*, are shown with SD. Circles indicate independent clones. **, P < 0.01 by two-sided Student's *t* test. Data are based on five independent clones.

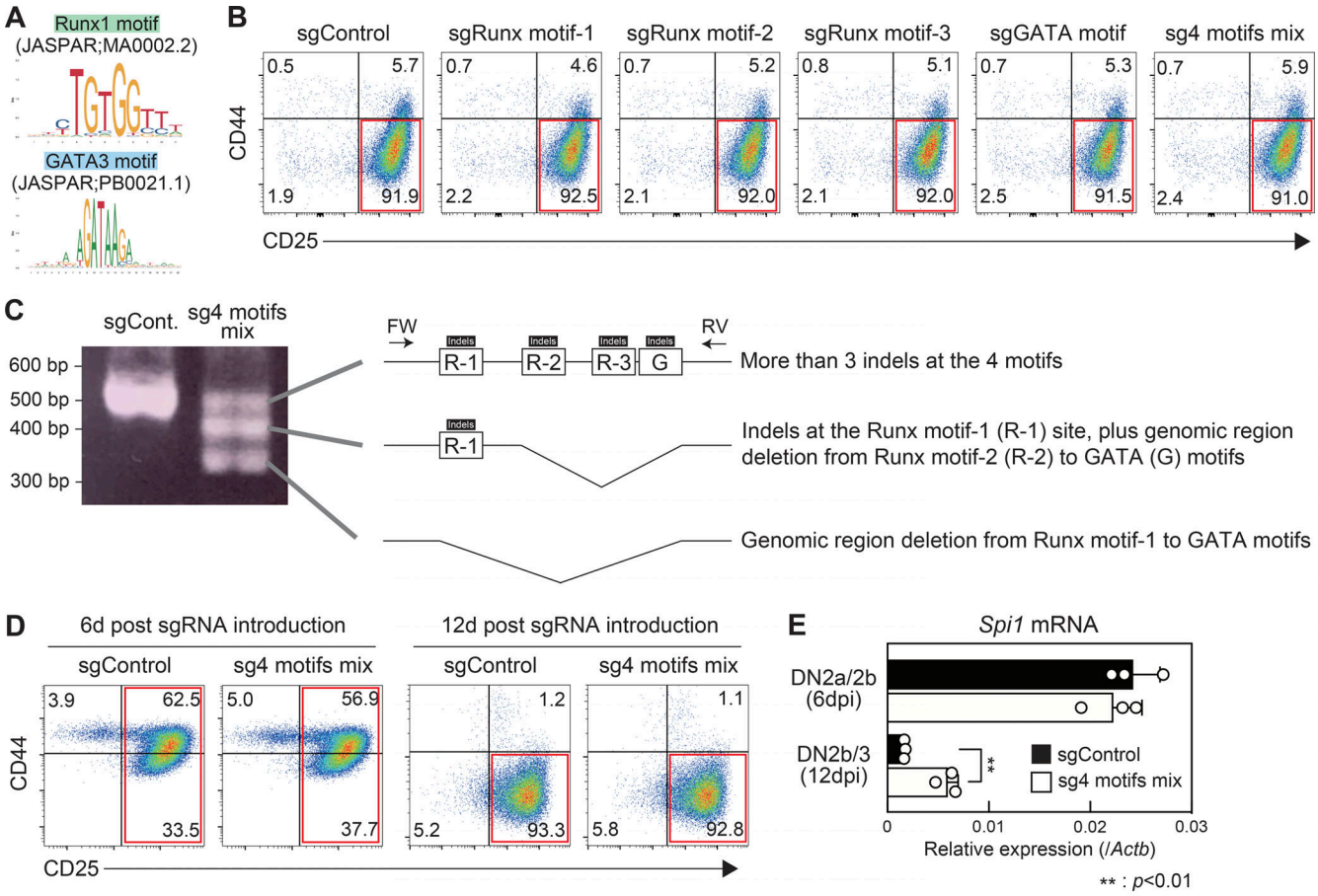

F GATA3 occupancy sites with different fixation conditions

	Promoters	ATAC open regions	Repeat sequence elements	Enrichment of GATA motif
FA crosslinked (n=36,288)	5.58%	18.6%	28.3%	*P*=1e-9426
DSG+FA crosslinked (n=36,479)	25.2%	64.5%	7.3%	*P*=1e-551

Figure S5. **Effects of mutations of the Runx and GATA motifs in the *Spi1* +3.7-kb element in primary pro–T cells. (A)** Runx1 (top) and GATA3 (bottom) motif sequence logos from JASPAR reference motif are shown. **(B)** Flow cytometric analyses of sgRNA-introduced Lin$^-$CD45$^+$CFP$^+$hNGFR$^+$ cells were performed as protocol B. Representative CD44/CD25 profiles are shown, with magenta rectangles indicating sorting gates. Results are representative of three independent experiments. **(C)** Mutation types induced in the +3.7-kb element by Cas9-mediated disruption using the sg4 motifs mix. Genomic DNA samples from the sgControl (sgCont.) or sg4 motifs mix–introduced Lin$^-$CD45$^+$CFP$^+$hNGFR$^+$ cells (B) were subjected to PCR analysis using FW and RV primers (indicated with arrows). The gel of PCR amplicons shows that different cells in the population experienced different extents of deletions. Each band was TA-cloned and sequenced and all were found to be altered from WT. Summary of mutations found in cells transduced with the sg4 motifs mix is shown. **(D)** Flow cytometric analyses of sgRNA-introduced Lin$^-$CD45$^+$CFP$^+$hNGFR$^+$ cells were performed using protocol D. Representative CD44/CD25 profiles 6 (left) or 12 (right) d after sgRNA infection are shown. CD25$^+$ (6 d) and CD44^{lo} (12 d) cells for sorting were labeled with red rectangles. Results are representative of three independent experiments. **(E)** sgRNA-introduced Lin$^-$CD45$^+$CD44$^+$CFP$^+$hNGFR$^+$ DN2a/2b cells and Lin$^-$CD45$^+$CD25$^+$CD44^{lo}CFP$^+$hNGFR$^+$ DN2b/3 cells were subjected to RT-qPCR analysis as protocol D. The relative expression levels (/*Actb*) of *Spi1* are shown with SD. **, P < 0.01 by two-sided Student's *t* test. Data are representative of two independent experiments and based on three biological replicates within an experiment. **(F)** Characterization of the GATA3 ChIP-seq peaks detected under different conditions of cross-linking. Percentages of GATA3 ChIP peaks from FA or DSG+FA (see Materials and methods) cross-linked DN2b/3 cells on promoters, ATAC-open regions, and repeat sequence elements and P values for enrichment of GATA motif are shown.

Table S1 is provided online as a separate Excel file and lists GATA3-interacting molecules in a pro–T cell-like cell line, Scid.adh.2c2.